

CENTRIFUGAL MICROFLUIDIC-BASED PLATFORMS FOR IN VITRO DIAGNOSTICS

**A Thesis Submitted to
the Graduate School of Engineering and Sciences of
İzmir Institute of Technology
in Partial Fulfillment of the Requirements for the Degree of
MASTER OF SCIENCE
in Bioengineering**

**by
Sadık KOÇ**

**July 2024
İZMİR**

We approve the thesis of **Sadık KOÇ**

Examining Committee Members:

Assoc. Prof. Dr. Hüseyin Cumhuri TEKİN

Department of Bioengineering, İzmir Institute of Technology

Assoc. Prof. Dr. Engin ÖZÇİVİCİ

Department of Bioengineering, İzmir Institute of Technology

Assoc. Prof. Dr. Sinan GÜVEN

Department of Medical Biology, Dokuz Eylül University

16 July 2024

Assoc. Prof. Dr. Hüseyin Cumhuri TEKİN

Supervisor, Department of Bioengineering, İzmir Institute of Technology

Assoc. Prof. Dr. Ceyda ÖKSEL

KARAKUŞ

Head of the Department of Bioengineering

Prof. Dr. Mehtap EANES

Dean of the Graduate School of

Engineering and Sciences

ACKNOWLEDGMENTS

I would like to thank everyone who supported and helped me throughout the preparation of this thesis.

First and foremost, I would like to express my deepest gratitude to my thesis advisor, Dr. Hüseyin Cumhuri TEKİN, for his invaluable guidance and support. His assistance made it possible for me to complete this work.

Special thanks to my friends at the LBMS lab, especially Büşra ERİMEZ, Seren KEÇİLİ, Cemre ÖKSÜZ, and Betül KARAKUZU. Working with you and sharing this journey has been truly enjoyable.

I would also like to thank my friends Berkan ŞİRİN, Beylem GİRGIN, and Merve ÜNAL, as well as our interns and my friends Hamza Erdem BOLAT and Furkan Bora CEHİZ. Your support and motivation have been incredibly valuable to me.

I am also grateful for the financial support provided by The Scientific and Technological Research Council of Turkey (TUBITAK) (Grant No. 22AG032), the scientific research project (2022-IYTE-2-0056) and TUBITAK (2210-C Domestic Priority Areas Master's Scholarship Program).

Additionally, I would like to thank IZTECH Center for Materials Research (CMR) for the measurements, Dr. Metin TANOĞLU for the contact angle measurements, Dr. Ceyda ÖKSEL KARAKUŞ, Dr. Devrim PESEN OKUR, and Dr. Özden YALÇIN ÖZUYSAL for their assistance. Special thanks to Sinan GÜVEN and Dr. İlhan GÜRSEL from Izmir Biomedicine and Genome Center for their help with nanoparticle measurements. I would also like to extend my thanks to Ramazan TEMİZKAN and Aslı KISIM for their assistance with the exosome experiments.

Finally, my heartfelt thanks go to my beloved family, my grandmother Fatma HALAÇ, my mom Serpil KOÇ and my dad Hüseyin KOÇ, for their financial and emotional support. Without their help, it would not have been possible to complete this work.

ABSTRACT

CENTRIFUGAL MICROFLUIDIC-BASED PLATFORMS FOR IN VITRO DIAGNOSTICS

In vitro diagnostics (IVDs) encompass all tools used in medical diagnosis and play a critical role in enabling early disease detection. The advancement of IVDs has led to the use of exosomes, which facilitate intercellular communication, as biomarkers for early diagnosis. Although traditional IVDs are considered the gold standard, they often come with high costs and lengthy processing times. To address these challenges, IVDs are being adapted to point-of-care systems using microfluidic technologies. In this context, a novel microfluidic fabrication method was developed to isolate and enrich exosomes on a poly(methyl methacrylate) (PMMA)-based microfluidic chip. This method leverages pure acetone as both a surface enhancer and adhesive, overcoming issues of surface roughness and opacity by promoting self-healing and transparency in the PMMA channels. The resulting chips are not only more durable but also cost-effective and easy to fabricate. This method was successfully applied to create a centrifugal microfluidic chip with a dead-end channel designed for nanoparticle and exosome isolation. The chip efficiently isolated particles of various sizes—200 nm in 20 minutes, 100 nm in 30 minutes, and 50 nm in 60 minutes—using a standard bench-top centrifuge at 9000 rpm (9418 g). Notably, exosomes were isolated from the cell medium within an hour without the need for markers. This innovative centrifugal-based microfluidic platform holds promise for diverse IVD applications.

ÖZET

İN VİTRO TEŞHİS İÇİN SANTRİFÜJ EDİLEBİLİR MİKROAKIŞKAN TEMELLİ SİSTEMLER

İN vitro tanı (IVD) yöntemleri, tanı koymak için kullanılan tüm araçları kapsarlar ve erken teşhis sağladıkları için büyük önem taşırlar. IVD'lerin gelişimi, hücreler arası iletişimi sağlayan eksozomların, özellikle hastalıkların erken teşhisinde biyomarker olarak kullanılmasına olanak tanımıştır. Geleneksel IVD'ler altın standart olarak kabul edilmesine rağmen, genellikle yüksek maliyetli ve zaman alıcıdır. Bu zorlukların üstesinden gelmek için IVD'lerin mikroakışkan sistemler kullanılarak hasta başı sistemlerine uyarlanması gerekmektedir. Bu bağlamda, polimetil metakrilat (PMMA) bazlı bir mikroakışkan çip üzerinde eksozomları izole etmek ve zenginleştirmek için yeni bir mikroakışkan üretim yöntemi geliştirilmiştir. Bu yöntemde, saf aseton hem yüzey iyileştirici hem de yapıştırıcı olarak kullanılmış, PMMA kanallarındaki yüzey pürüzlülüğü ve opaklık sorunlarını ortadan kaldırarak yüzeyin kendini onarmasını ve şeffaf hale gelmesini sağlamıştır. Elde edilen çipler, yalnızca daha dayanıklı olmakla kalmayıp, aynı zamanda uygun maliyetli ve kolay üretilebilir niteliktedir. Bu yöntem, nanoparçacık ve eksozom izolasyonu için kapalı bir kanal içeren santrifüjlü mikroakışkan bir çip üretmek için başarıyla uygulanmıştır. Çip, 9000 rpm (9418 g) hızında standart bir masaüstü santrifüjde 200 nm parçacıkları 20 dakikada, 100 nm parçacıkları 30 dakikada ve 50 nm parçacıkları 60 dakikada izole etmeyi başarmıştır. Özellikle, eksozomlar, belirteç kullanmadan, hücre ortamından bir saat içinde izole edilmiştir. Bu yenilikçi santrifüj tabanlı mikroakışkan platform, farklı IVD uygulamaları için umut vaat etmektedir.

TABLE OF CONTENTS

LIST OF FIGURES.....	viii
LIST OF TABLES.....	x
ABBREVIATIONS.....	xi
CHAPTER 1 INTRODUCTION	1
1.1. In Vitro Diagnostics.....	1
1.2. Microfluidic Technology for In Vitro Diagnostics.....	2
1.3. Centrifugal Microfluidics	4
1.4. Aim of the Thesis.....	6
CHAPTER 2 FABRICATION OF PMMA-BASED MICROFLUIDIC DEVICES USING PURE ACETONE AS A SURFACE ENHANCEMENT AND BONDING AGENT.....	7
2.1. Introduction.....	7
2.2. State-of-the-Art of PMMA-Based Microfluidic Fabrication Techniques	10
2.2.1. Fabrication of Microfluidic Channels.....	10
2.2.1.1. Hot Embossing.....	11
2.2.1.2. Injection Molding.....	11
2.2.1.3 Micromachining.....	11
2.2.1.4. Laser Ablation.....	12
2.2.2. Channel Bonding	12
2.2.2.1. Thermal Bonding.....	13
2.2.2.2. Solvent Bonding.....	13
2.2.2.3. Adhesive Bonding.....	14
2.2.2.4. Other Bondings.....	15
2.3. Materials and Methods.....	15
2.3.1. Fabrication of Open Microfluidic Channels with Enhanced Channel Surface on PMMA	15
2.3.2. Bonding of PMMA Layers	17
2.3.3. Fabrication of Monolithic Microfluidic Chips.....	18
2.4. Statistical Analysis.....	18

2.5. Results.....	18
2.5.1. Effect of the Acetone Treatment on Open Microfluidic Channels	18
2.5.2. Characterization of PMMA Bonding.....	22
2.5.3. Fabricated Monolithic Microfluidic Devices.....	24
2.6. Comparison with Different Treatment and Bonding Methods	27
2.7. Conclusion	29
CHAPTER 3 ISOLATION AND ENRICHMENT OF EXOSOMES WITH CENTRIFUGAL MICROFLUIDIC DEVICE	30
3.1. Introduction.....	30
3.2. State-of-the-Art of Exosome Isolation.....	30
3.2.1 Conventional Methods for Exosome Isolation	32
3.2.1.1 Separation via External Field.....	32
3.2.1.2 Sieving Method.....	33
3.2.1.3. Colloidal Stability	33
3.3. Microfluidic Technologies for Exosome Isolation	34
3.3.1. Centrifugal Microfluidics for Exosome Isolation	34
3.4. Materials and Methods.....	37
3.4.1. Fabrication of Falcon Tubes Compatible with Bench-Top Centrifuge	37
3.4.2. Fabrication of Microfluidic Chip for Nanoparticle Isolation and Collection.....	38
3.4.3. Characterization and Collection of Nanoparticles	40
3.4.4. Preparation of Isolated Exosomes.....	42
3.4.5. Preparation of Conditioned Medium Exosomes	42
3.5. Statistical Analysis.....	43
3.6. Results.....	43
3.6.1. Movement of Nanoparticles in the Channel Depending on Time	43
3.6.2. Enrichment of Nanoparticles at the Bottom of the Channel.....	48
3.6.3. Collection of Enriched Nanoparticles	49
3.6.4. Isolation of Exosomes.....	50
3.7. Conclusion	52
CHAPTER 4 CONCLUSION	54
REFERENCES.....	56

LIST OF FIGURES

<u>Figure</u>	<u>Page</u>
Figure 1.1. Illustration of conventional IVDs.	3
Figure 1.2. Microfluidic devices for IVDS.	4
Figure 1.3. Commercially available centrifugal microfluidic devices for IVDs.	5
Figure 2.1. Illustration of the conventional microfluidic fabrication.	8
Figure 2.2. Illustration of the methods for creating microfluidic channel geometries. ..	10
Figure 2.3. Illustration of the bonding techniques.	14
Figure 2.4. Illustration of the fabrication of PMMA-based microfluidic channel with enhanced optical clarity.	16
Figure 2.5. Illustration of the bonding protocol.	17
Figure 2.6. Effects of acetone temperature, time in acetone (3 and 5 min) and 100°C oven waiting time (5, 10 and 15 min) on surface healing.	19
Figure 2.7. SEM of microfluidic channel surfaces engraved on PMMA.	20
Figure 2.8. Light transmittance values of bulk, engraved, and engraved and then treated PMMA pieces for different wavelengths.	21
Figure 2.9. Contact angle measurement of the PMMA surfaces.	22
Figure 2.10. The effect of acetone concentration and temperature treatment time on bonding strength.	23
Figure 2.11. Bubble formation on the bonding surfaces after 5 min heat treatment at 100°C.	24
Figure 2.12. SEM of cross-section views of bonded channels.	25
Figure 2.13. Microfluidic channel fabrication using the bonding method.	26
Figure 2.14. Time-lapse images capturing the evolution of microfluidic channels filled with a red food color solution over a 72-hour inspection period. The channels' inlets and outlets were sealed either by placing a PMMA piece over them, clamping the piece onto the chip, or bonding it to the chip.	27
Figure 3.1. TEM images of the exosomes.	31
Figure 3.2. Centrifugal microfluidic devices for exosome isolation.	35
Figure 3.3. Illustration of the acting forces on a centrifugal microfluidic.	38

<u>Figure</u>	<u>Page</u>
Figure 3.4. Image of the 3D printed falcon tubes that is compatible with bench-top centrifuge device.	38
Figure 3.5. Microfluidic chips used in nanoparticle and exosome isolation.	39
Figure 3.6. Isolation and the enrichment protocol for the nanoparticles.	40
Figure 3.7. Microscope images showing analysis zones.	41
Figure 3.8. Collection protocol of the isolated particles.	41
Figure 3.9. Collection protocol of the conditioned medium exosomes.	43
Figure 3.10. Microscope image of 200 nm particles aggregating in the time-dependent channel at 9000 rpm.	44
Figure 3.11. Microscope image of 100 nm particles aggregating in the time-dependent channel at 9000 rpm.	45
Figure 3.12. Microscope image of 50 nm particles aggregating in the time-dependent channel at 9000 rpm.	46
Figure 3.13. Before and after centrifuging PBS used as control for 60 min at 9000 rpm.	47
Figure 3.14. ImageJ analysis of the 8 zones of the chip.	48
Figure 3.15. Change of mean intensity value of the channel bottom depending on time (mean intensity value of PBS noise is subtracted).	49
Figure 3.16. Fluorescence microscope image of the isolated particles before and after collection from the channel.	50
Figure 3.17. Images of the channel bottom under confocal microscopy before and after centrifugation.	51
Figure 3.18. ImageJ analysis of the top and bottom of the chip before and after centrifuging for 60 min at 9000 rpm.	51
Figure 3.19. ImageJ analysis of the top and bottom of the chip before and after centrifuging for 60 min at 9000 rpm.	52

LIST OF TABLES

<u>Table</u>	<u>Page</u>
Table 2.1. Comparison Between Several Surface Enhancement and Bonding Techniques for the Fabrication of PMMA-Based Microfluidics.	28

ABBREVIATIONS

FDA	Food and Drug Administration
IVD	In Vitro Diagnostics
ELISA	Enzyme-Linked Immunosorbent Assay
PCR	Polymerase Chain Reaction
MS	Mass Spectrometry
POC	Point-of-Care
MEMS	Microelectromechanical Systems
PDMS	Polydimethylsiloxane
PMMA	Poly(methyl methacrylate)
COC	Cyclic olefin copolymer
PC	Polycarbonate
CNC	Computer Numerical Control
EVs	Extracellular Vesicles
SFM	Serum Free Medium

CHAPTER 1

INTRODUCTION

1.1. In Vitro Diagnostics

According to the Food and Drug Administration (FDA), all devices and reagents used in the collection, preparation, and analysis of biological samples such as sweat, saliva, and tissue are called in vitro diagnostic (IVD).¹ With today's developing technology, it is also called the doctor's eye because it provides a specific diagnosis of the disease using various biomarkers in the clinic.² In addition to diagnosing the disease, monitoring, treatment, and post-treatment processes are also provided.³ In addition, since IVD does not require direct contact with the human body (saliva, urine, etc.) or minimally invasive procedures (such as blood) to collect samples, it does not have the biosafety concerns of in vivo methods.⁴ Thanks to these advantages and importance, the market share of IVD technologies, whose market share is increasing day by day, has reached 74.46 billion dollars globally in 2022.⁵

IVD methods such as enzyme-linked immuno surface assay (ELISA), polymerase chain reaction (PCR), and mass spectroscopy (MS), which are used today and have become the gold standard, are used in many areas from the pharmaceutical industry to the diagnosis of parasitic diseases and infectious diseases.⁶ However, these methods have disadvantages such as multiple sample preparation steps, the use of expensive and complex devices, being time-consuming, and the need for trained personnel.⁷ Considering the importance of IVD systems, it is necessary to make this technology accessible to people in a quality and cost-effective manner, especially in regions with limited resources.⁸ To achieve this, traditional IVD methods need to be adapted to point-of-care (POC) systems, miniaturized, and made portable.⁹

Developments in the field of IVD tests have enabled the use of new biomarkers, especially for the detection of diseases at early stages such as cancer.¹⁰ Exosomes are nano-sized particles that are released from most of the cells and play a critical role in

intercellular communication with the nucleic acids they contain.¹¹ Since it is possible to access exosomes from almost all body fluids (such as sweat and saliva), it has the potential to be used as a non-invasive marker for cancer diagnosis.¹² Since exosomes have just begun to be used in the field of IVD, there is no traditional method.¹³ Although exosomes can be isolated by methods such as ultracentrifugation and nanofiltration, these methods are time-consuming, expensive, and low in efficiency.¹⁴ For this reason, new methods and technologies are needed for the isolation of exosomes.

1.2. Microfluidic Technology for In Vitro Diagnostics

POC systems, which enable healthcare services to be provided at or close to the patient, have an important place as they provide early diagnosis and disease follow-up.¹⁵ Especially in the SARS-CoV-2 pandemic that occurred in recent years, it has been the biggest indicator of the need for POC systems to monitor and prevent the disease.¹⁶ When developing POC systems, attention should be paid to features such as reliability, portability, simplicity, and performing the process from sample to result on a single device.¹⁷ For this reason, microfluidic technology has an important place in the development of POC systems.¹⁸

Microelectromechanical systems (MEMS) are technologies that have existed for more than 30 years and are also called microfabrication, laboratory-on-chip, microsystems, micro total analysis systems.¹⁹ Microfluidics, a branch of MEMS It is a technology that allows the processes carried out in the laboratory environment to be carried out in micrometer-sized channels.²⁰ Thanks to the design and control of experiments at the micrometer scale, this technology has enabled the miniaturization of IVD systems due to the many advantages it offers in studies in the field of biology.^{3,21} Microfluidic systems can perform many operations such as sample preparation (filtration, etc.), manipulation, and analysis of the reagent and sample in a very small area and volume.²²

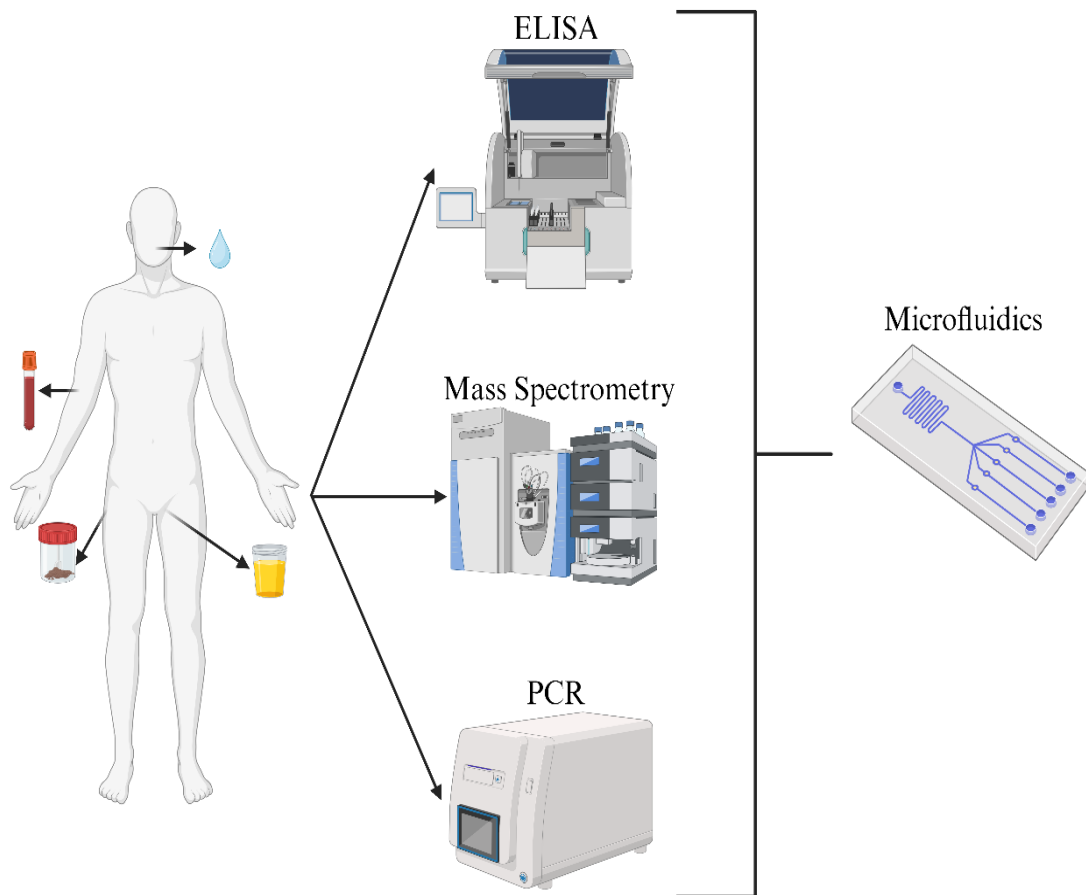


Figure 1.1. Illustration of conventional IVDs.

Thanks to the adaptation of IVDs to microfluidics, operations normally performed on devices such as ELISA and PCR can now be performed on microfluidic chips (Figure 1.1) In addition, with the developed systems, diseases such as chlamydia, malaria, and thyroid disorder can be diagnosed (Figure 1.2).²⁵⁻²⁷

However, while these methods are being developed, performing all operations (sample preparation, centrifugation, filtration, analysis, etc.) on a single chip is still a major obstacle. Additionally, as chip complexity increases, microfluidic chip fabrication becomes more difficult, and its cost increases. For this reason, new fabrication techniques and different microfluidics technologies such as centrifugal microfluidics are needed.²⁸

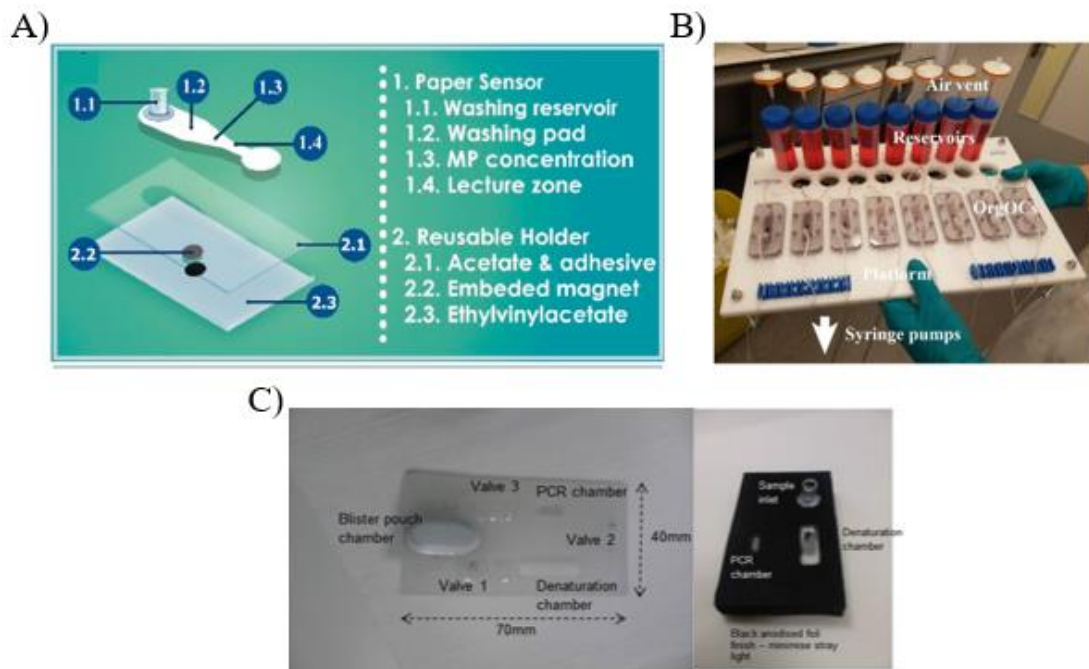


Figure 1.2. Microfluidic devices for IVDS. A) Paper-based microfluidic for quantitative malaria detection (Source: Arias-Alpízar et al., 2022) B) Microfluidic system for thyroid detection (Source: Carvalho et al., 2023). C) Microfluidic real-time PCR system for *Chlamydia trachomatis* detection (Source: Brennan et al., 2021).

1.3. Centrifugal Microfluidics

Microfluidic systems can be divided into two classes, active and passive systems, based on the forces used for fluid manipulation.²⁹ While active systems include systems that require an additional external force such as centrifugal, electrokinetic, and magnetic, passive systems include systems that use internal forces such as capillary force based on channel geometry and hydrodynamic forces.³⁰ Centrifugal microfluidics or Lab-on-a-disc platforms, which are a branch of active microfluidic systems, provide liquid manipulation by utilizing centrifugal force.²⁸ This technology facilitates the adaptation of IVD systems to microfluidic technologies, as mixing the sample with the reagent, metering, and integrating the chip with optical systems are easy.³¹ Centrifugal force, just like a gravitational force, applies a force to every area of the chip, always from the center out.³²

By taking advantage of this phenomenon, unlike normal microfluidics, it provides liquid transfer without the need for devices such as external syringe pumps and vacuum. In addition, mixing and valve structures are integrated into the chip and a sharper liquid manipulation can be achieved with this technology.³³ In addition, due to the effective and equal force applied to the chip, problems such as bubble formation in the channel are minimized.³⁴ Owing to these advantages, companies such as Roche and 3M have adopted this technology and centrifugal microfluidic systems, which are actively used in the market, have been developed (Figure 1.3).³³

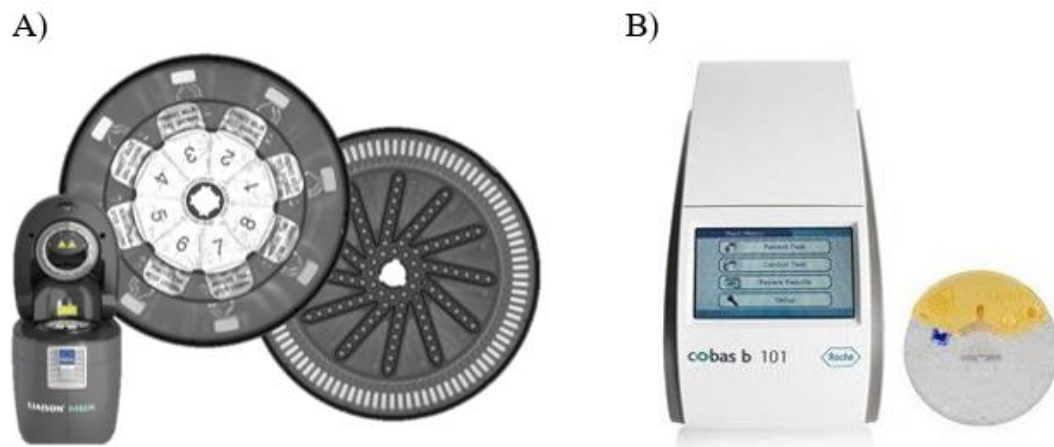


Figure 1.3. Commercially available centrifugal microfluidic devices for IVDs. A) LIAISON MDX for real-time PCR (Source: DiaSorin, 2024). B) Cobas b 101 for blood parameter analysis (Source: Roche, 2024).

Since centrifugal microfluidics are often produced from polycarbonate materials, they can work seamlessly with different solutions, surfactants, and biological fluids.³⁵ Thanks to centrifugal force, it can provide isolation and enrichment of small amounts of cells, particles, and molecules in these liquids by taking advantage of their physical properties (density, volume, etc.).³⁶ In order for these processes to occur, the forces acting on the liquid must be thoroughly understood and parameters such as channel design and centrifugal force and time must be carefully optimized.³⁷

1.4. Aim of the Thesis

The aim of this thesis is to develop and optimize a poly(methyl methacrylate) (PMMA)-based centrifugal microfluidic chip for the efficient isolation and enrichment of exosomes. The newly designed chip incorporates a novel microfluidic fabrication method that utilizes pure acetone for both enhancing surface quality and bonding PMMA layers. This approach addresses issues related to surface roughness and opacity, resulting in a durable, cost-effective, and easy-to-manufacture device. The chip demonstrates effective isolation of exosomes from cell medium within one hour, with the capability to handle various nanoparticle sizes. The advancement of this microfluidic technology is expected to enhance the integration of exosomes into in vitro diagnostic systems, improving biomarker potential and facilitating the extraction of exosomes from body fluids for future applications.

CHAPTER 2

FABRICATION OF PMMA-BASED MICROFLUIDIC DEVICES USING PURE ACETONE AS A SURFACE ENHANCEMENT AND BONDING AGENT

2.1. Introduction

Owing to advances in microfluidics, IVDs can be adapted to POC systems.³⁸ However, fabrication is of great importance in order to increase the applicability and accessibility of these systems.³⁹ Especially in poor and inaccessible regions of the world, since resources such as clean water and electricity, which are the most basic needs, are limited, attention should be paid to the development and use of sustainable, low-cost, easily produced fabrication techniques when developing microfluidic systems.⁴⁰

Glass and Polydimethylsiloxane (PDMS) are widely used materials in microfluidics fabrication because of their physical and chemical versatility.⁴¹ PDMS-based microfluidics are one of the most popular used microfluidic fabrication techniques.⁴² In this technique, after PDMS is mixed with a heat and light activating agent to solidify, it is poured onto a master mold with the desired channel geometry and waited for it to cure.⁴³ PDMS, which is removed from the mold after curing, is produced by applying processes such as oxygen plasma to close the open channels, often by adhering it to a glass substrate.⁴⁴ While PDMS molds can be produced with 3D printers, they are traditionally produced by photolithographic method on a silicon wafer.⁴⁵ It is spread by spinning photoresist (usually SU-8) onto silicon.⁴⁶ The silicon wafer placed under the mask made of plastic or glass containing the channel geometry is exposed to UV light and the photoresist solidifies.⁴⁷ The parts that do not solidify are removed by washing in

developer and a positive or negative mold of the desired channel geometry is created (Figure 2.1).³⁰

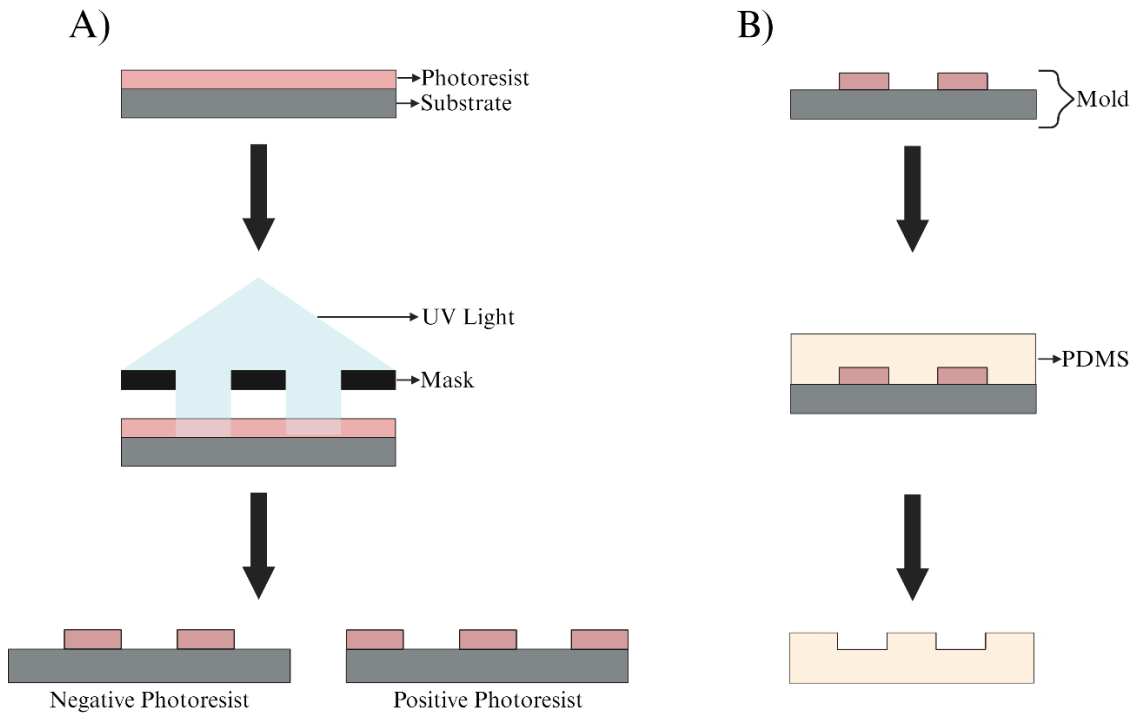


Figure 2.1. Illustration of the conventional microfluidic fabrication. A) Master mold fabrication for PDMS. The photoresist is spun and spread on the substrate. It is exposed to UV light under a mask with channel geometry. Mold fabrication is completed by removing the uncured resist with the developer. B) Creation of PDMS channels. PDMS mixed with a curing agent is transferred onto the mold and spun. After PDMS is cured with heat, it is removed from the mold and the channel pattern in the mold is transferred to PDMS.

Since the fabrication techniques for these materials often require the use of a silicon-based master mold, they require high costs, complex fabrication steps, and clean room facilities.⁴⁸ Oligomers in PDMS do not have crosslinks and may cause problems in cell applications, and chips produced with PDMS are not suitable for the fabrication of centrifugal microfluidic systems because they have low strength.⁴⁹ In addition, this

fabrication method is useful in conventional microfluidics, it is very difficult to use it in centrifugal microfluidics due to the low strength of PDMS and the glass substrate used.³⁴ For this reason, polymers like PMMA, cyclic olefin copolymer (COC), and polycarbonate (PC) are used in the fabrication of centrifugal microfluidics.⁵⁰ Durable microfluidic chips can be produced with materials processed using methods such as micromachining and polymer molding.⁵¹

Thermoplastic polymer materials have begun to be widely used in microfluidic chip fabrication due to their low cost, easy processability, and versatile material properties.⁵² Thanks to these features, they are more suitable for mass fabrication compared to glass or silicon-based systems.⁵³ Many polymers such as PMMA, COC, and PC can be used as alternatives to glass and silicone.⁵⁴

PMMA is one of the most commonly used polymers in microfluidic chip fabrication.⁵⁵ It has very favorable properties with its low cost, optical transparency, low autofluorescence, mechanical properties, and biocompatibility.⁵⁶ It is also one of the polymers with the lowest hydrophobicity compared to other polymers.⁵⁵ There are various techniques for PMMA-based microfluidics fabrication.

In this chapter, PMMA-based microfluidic chip fabrication technique was developed by using pure acetone as both a surface enhancer and bonding agent. The channels were kept in pure acetone at 50 °C for 3 min, and the glass transition temperature of PMMA was subjected to heat treatment for 15 min in an oven at 100 °C, allowing the channel surfaces to heal themselves. In this way, the channel surface, which was damaged by the laser process, was made smooth and transparent again, and PMMA bulk properties were restored. Subsequently, after the open channels and another PMMA layer were attached with clips, pure acetone was administered between the PMMA sheets with a capillary effect and adhesion was achieved by heat treatment in an oven at 100 °C for 5 min. At the end of the bonding process, a high-strength (>30 MPa) and air-tight seal is achieved. With this work, fast, easy, low-cost, and high-strength chip fabrication has become possible with the help of a single solvent. It is hoped that this method will facilitate the development of microfluidic systems that can be used in IVD.

2.2. State-of-the-Art of PMMA-Based Microfluidic Fabrication Techniques

PMMA-based microfluidic fabrication can be divided into two classes: processing the desired channel geometries on the material surface and bonding the created open channels with another PMMA layer.⁵⁷

2.2.1. Fabrication of Microfluidic Channels

In microfluidic chip fabrication with PMMA, channels are fabricated by machining on the surface. Channels on PMMA can be made by hot embossing, injection molding, micromachining, and laser ablation methods (Figure 2.2).

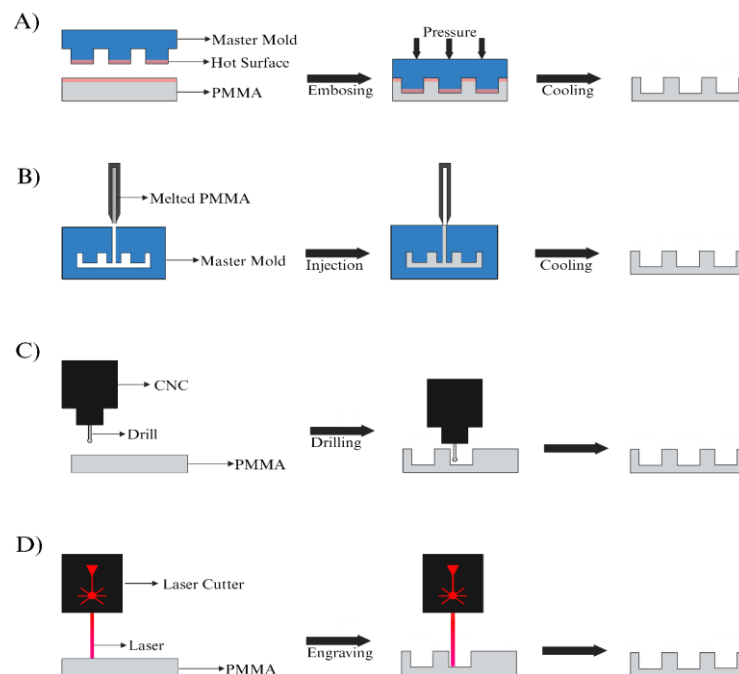


Figure 2.2. Illustration of the methods for creating microfluidic channel geometries. A) Hot embossing. B) Injection molding. C) Micromachining. D) Laser ablation.

2.2.1.1. Hot Embossing

The hot embossing method is a widely used method for the mass fabrication of PMMA-based microfluidics.⁵⁸ In this method, a metal or silicone mold containing the channel geometry is raised above the glass transition temperature of PMMA ($>105^{\circ}\text{C}$) and pressed to the material surface at high pressures, thus transferring the channel geometry on the mold to the material surface.⁵⁹ Depending on the materials and equipment used, fabrication can be achieved in 2-20 min.⁶⁰ For example, electrophoresis chips can be produced by hot embossing nickel strings at 180°C onto PMMA.⁶¹ However, these methods require a master mold, the fabrication of channels with a high aspect ratio is difficult, and the material may break when the mold is separated from the material.

2.2.1.2. Injection Molding

It is widely used in the fabrication of microfluidic channels with PMMA.⁶² Powdered PMMA is injected into the mold with the channel geometry through a narrow opening at high temperature ($>105^{\circ}\text{C}$) and high pressure.⁶³ PMMA, which melts and combines in the mold, is removed from the mold when it drops below the glass transition temperature and PMMA parts with channel geometry are obtained. These processes occur quickly (<5 min). For example, droplet generators and mixing structures can be produced quickly.⁶⁴ However, the equipment used in this method is quite expensive and requires a master mold.⁶⁵

2.2.1.3. Micromachining

Micromachining is based on carving the surface with a drill bit using devices such as Computer Numerical Control (CNC).⁶⁶ For example, serpentine channels with

dimensions of 200 μm wide and 50 μm deep can be produced quickly.⁶⁷ However, in this method, the surface quality and optical properties are low and expensive.

2.2.1.4. Laser Ablation

Laser ablation is commonly used to create channels on PMMA.⁶⁸ In this method, a high-energy beam breaks the bonds of polymer molecules on the surface, leaving decomposed fragments from the ablation regions.⁶⁹ The laser, which generally moves in the x-y plane, processes the channels designed with computer-aided drawing programs onto the material.⁷⁰ Channel dimensions can be easily changed by changing the power and speed of the laser.⁷¹ In this method, as in micro-machining methods, surface quality and optical properties are low.⁷² Additionally, surface improvement processes can be expensive.⁵⁴

For this reason, methods have been developed to improve the surface in a cost-effective and rapid way. As an example, it has been noted that maintaining the PMMA in 23% acetone prepared in ethanol at 60°C for 10 min can result in improved laser-engraved surfaces.⁷³ In addition to soaking in acetone, surfaces can be treated by exposing PMMA layers to acetone vapor for 5 min and then curing them for 20 min to enhance the laser engraved surfaces.⁷⁴ Aside from acetone, a microfluidic chip may be created by enhancing the PMMA surface with chloroform vapor for 4 min.⁷⁵

2.2.2. Channel Bonding

The upper surface of channels machined on PMMA is often open.⁷⁶ For this reason, chip fabrication is achieved by covering the channels with an additional PMMA layer, taking care not to block the channels.⁵⁵ Oxygen plasma and corona treatment processes used in adhering PDMS to the glass surface, which are used in traditional microfluidics fabrication, cannot be used on thermoplastics because they provide very low adhesion strength.⁷⁷ In addition, processes such as oxygen plasma may cause the

emergence of highly cytotoxic by-products (hydrogen peroxide) on the surface.⁷⁸ Thermal bonding, solvent bonding, and adhesive bonding are used to bond PMMA layers (Figure 2.3).

2.2.2.1. Thermal Bonding

In this technique, PMMA layers heated above the glass transition temperature are pressed together with hydraulic pressure. With this method, bonding strength ranging from 1 MPa to 10 MPa can be obtained.⁷⁹ For example, a chip that performs electrophoretic separation was fabricated.⁸⁰ However, with this method, deformation may occur in the channels due to the high and pressure applied during fabrication.

2.2.2.2. Solvent Bonding

It is based on the bonding of the layers by re-establishing the opened bonds after the solvent applied to the interface of two PMMA layers causes the polymer bonds on the surface to be opened.⁸¹ It is possible to change the bonding strength by adjusting the solvent concentration and bonding time.⁸² Solvent duration and concentration must be adjusted well to avoid any deformation in the channels due to solvent.⁸³ For instance, by mixing 20% dichloromethane in 80% isopropanol, bonding with a strength of 4.2 MPa was achieved after curing for 15 min at 70°C.⁸⁴ Bonding of PMMA surfaces also can be achieved with a bonding strength of 3.48 MPa for ethanol and 6.21 MPa for isopropanol (IPA) by keeping it in ethanol or IPA for 5 min at 70 degrees and then using it between cleaned surfaces.⁸⁵ In another method, after applying ethanol or IPA directly to the surfaces, an adhesion with a strength of 28.75 MPa can be achieved after keeping the surfaces attached to each other with the help of clips in the oven for 10 min (74°C for ethanol, 68°C for IPA) and then for 40 min at room temperature.⁷⁹ Furthermore, a solvent-based bonding technique using acetic acid and UV irradiation can help to reach 11.75 MPa bonding strength with 20 min curing.⁸⁶

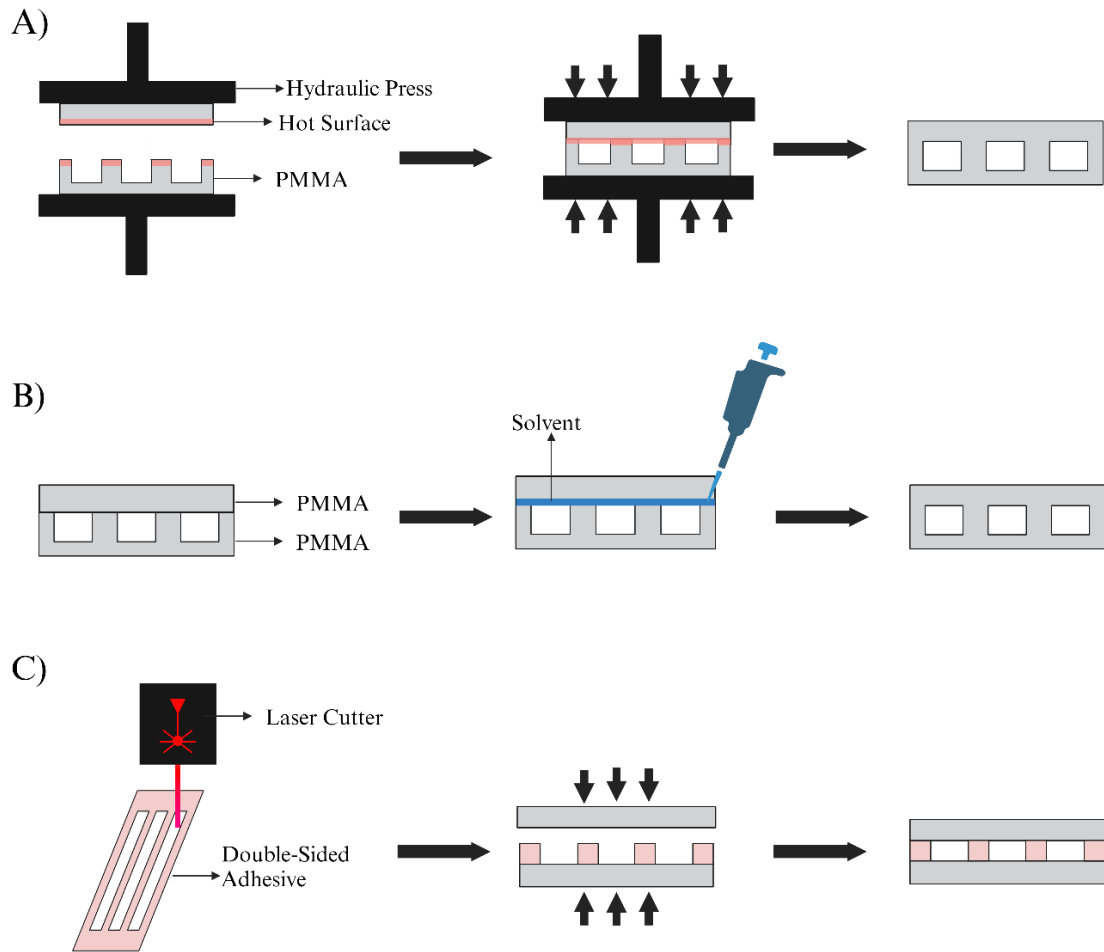


Figure 2.3. Illustration of the bonding techniques. A) Thermal bonding. B) Solvent bonding. C) Adhesive bonding.

2.2.2.3. Adhesive Bonding

It is a method of bonding PMMA layers with pressure-sensitive silicone or acrylic-based double-sided adhesive tapes. After the desired channel geometry is created on the tape with a laser cutter, when two PMMA layers are glued together, channels at the tape height can be obtained.⁸⁷ For example, microfluidic chips that selectively quantify white blood cells and neutrophils can be produced with channels of 4 mm width and 50 μm height.⁸⁸ Thanks to the tapes, multilayer microfluidics can be produced

without damaging transparency.⁸⁹ In this method, bonding strength ranging from 1 MPa to 2 MPa can be obtained. In addition, channel height is limited by the size of the band.⁹⁰

2.2.2.4. Other Bondings

There are methods for bonding PMMA parts using microwaves.⁹¹ It can provide rapid bonding by absorbing microwave rays of a thin metal sheet (such as gold) between two PMMA sheets.⁹² For example, it has been shown that an eye-shaped metallic mesh can be placed between PMMA layers, and the layers can be bonded via microwave.⁹³ It has also been shown that microwave adhesion can be achieved by spreading a 50% concentration of ethanol between PMMA layers, without the need for a metal between the PMMA layers.⁹¹

2.3. Materials and Methods

2.3.1. Fabrication of Open Microfluidic Channels with Enhanced Channel Surface on PMMA

1 mm × 10 mm (width × length) channels were engraved on the surface of PMMA (Akpolimer, Turkey) with a thickness of 2 mm using a laser cutter equipped with a 40W CO₂ laser (Makeblock LaserBox, China). Before engraving, the front and back surfaces of the PMMA were covered with tape (Avansas, Turkey). The channel template was cut from the tape with the laser cutter by adjusting the cutting speed to 80 mm.s⁻¹ (100%) and the laser beam power to 20W (%50). After cleaning the surface with isopropanol (Luxor Chemicals, Turkey), engraving was started. Channel depth of 150 μm was achieved by adjusting the engraving speed to 330 mm.s⁻¹ and the laser beam power to 40W (100%). Afterwards, the engraved channels were kept in pure acetone (Stein Chemicals, Turkey) at 50 °C for 3 min to enhance the optical clarity of PMMA. The tape was used to protect

underlying PMMA from acetone treatment. Then, as a final step, the channels were treated in an oven (Memmert, Germany) at 100 °C for 15 min for heat treatment. After the heat treatment, the protective tape layers were removed. With this procedure, the open microfluidic channels were ready for use (Figure 2.4).

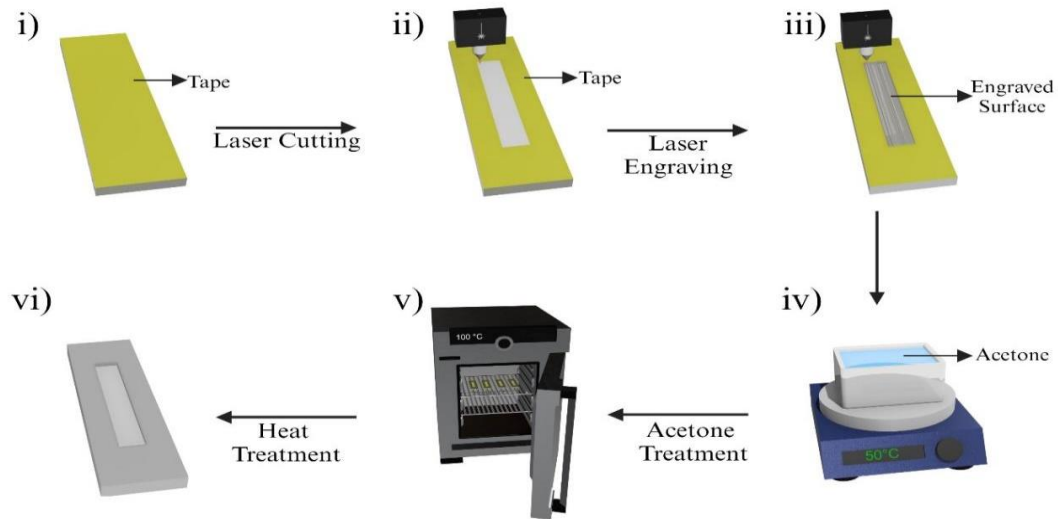


Figure 2.4. Illustration of the fabrication of PMMA-based microfluidic channel with enhanced optical clarity. (i) The PMMA surface is covered with tape to prevent unwanted acetone damage to the material. (ii) The channel template was cut from the tape with the laser cutter then the access tape on the channel template was removed. (iii) The Channel is engraved on the surface of the PMMA using a laser cutter. (iv) Engraved PMMA is placed in a 50°C acetone solution for 3 min. (v) Engraved PMMA was treated at 100°C for 15 min. (vi) Open microfluidic channel is now ready for use.

For the characterization of the engraved surfaces, surfaces were examined with Fei Quanta 250 Scanning Electron Microscopy (SEM) (Thermo Fisher, USA). A spectrometer (HR4000CG UV-NIR, Ocean Optics, USA) was used for the measurement of transmission values of the surfaces for the evaluation of the optical clarity. Contact angles of the surfaces were measured using Attention Optical Tensiometer (KSV Instruments, USA).

2.3.2. Bonding of PMMA Layers

To evaluate the PMMA bonding strength, 25 mm × 75 mm PMMA pieces with a thickness of 3 mm were washed with 10% isopropanol and dried with nitrogen gas. Then, PMMAs were brought together to overlap with each other 25×25 mm in area and fixed using 4-piece 15 mm binder clips (Avansas, Turkey) to create pressure on the bonding surface. After 100 μ L of acetone solution (50-100% prepared in distilled water) was spread on the bonding surface using capillary effects with pipetting, PMMA pieces were incubated at 100 °C, which is the glass transition temperature of PMMA⁹⁴, for 5-15 min (Figure 2.5). A lap-shear test was applied on to these bonded PMMA pieces at 0.5 mm/min speed to evaluate bonding strength. Bonding areas were examined under a Zeiss Axio Vert A1 inverted fluorescence microscope (ZEISS, Switzerland) to observe bubble formation inside the bonded area. Cross-sections of the bonded areas were also examined under Fei Quanta 250 Scanning Electron Microscopy (Thermo Fischer, USA).

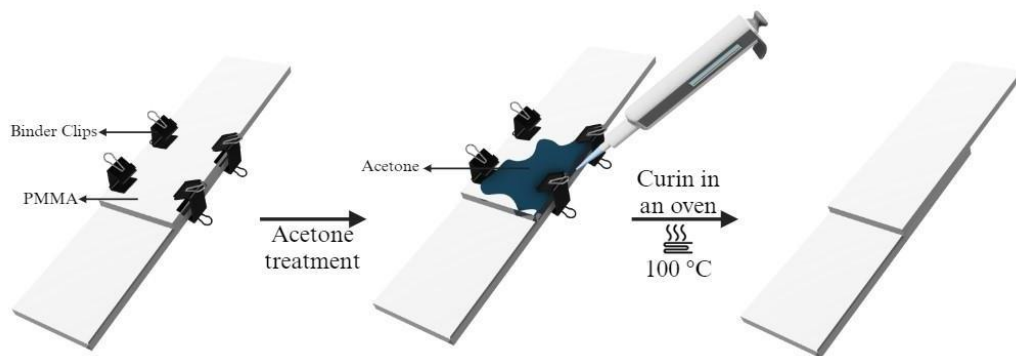


Figure 2.5. Illustration of the bonding protocol. (i) First, PMMA pieces were fixed on top of each other with binder clips. (i) Then, an acetone solution was spread between PMMA pieces. (iii) Afterwards, a temperature-treatment at 100°C was applied for bonding of PMMA pieces.

2.3.3. Fabrication of Monolithic Microfluidic Chips

Monolithic microfluidic chips with 1x10 mm (width x length) and 150 μ m channel depth were produced in order to demonstrate the ability of surface healing and bonding to be used in harmony with each other to produce a microfluidic chip. Vertical sections were taken from the fabricated chips, and the channel sections were examined with a Fei Quanta 250 Scanning Electron Microscopy (Thermo Fisher, USA), bonded without treatment, treated only in acetone at 50°C for 3 min, and heated only in an oven at 100°C for 15 min. compared with treated channel sections. The smallest channel sizes that can be produced with this method were also produced and examined under a Zeiss Axio Vert A1 inverted fluorescence microscope (ZEISS, Switzerland). Additionally, the seal of the bonding was also analyzed for leakage and evaporation.

2.4. Statistical Analysis

Data were presented as the mean \pm standard deviation (SD) of at least three replications of studies. Two-way ANOVA combined with Tukey's multiple comparison test was used to statistically analyze the data. These analyses were carried out using GraphPad software (Prism 8 version, GraphPad, USA).

2.5. Results

2.5.1. Effect of the Acetone Treatment on Open Microfluidic Channels

Before surface characterization, the engraved channels were kept in acetone at room temperature (25 °C) and acetone close to the boiling point (50 °C) for 3 and 5 min, and then in an oven at 100 °C for 5-10-15 min, and the surfaces were examined under a

microscope (Figure 2.6). Since the effect of acetone will be maximum at the boiling point, this temperature was chosen and compared with room temperature. In addition, different periods were tested within 100 °C, where 100 °C is the glass transition temperature for PMMA and the thermal effect will have the maximum effect on solid state PMMA. As a result of our observations, it was observed that acetone had no effect on surface improvement in both periods at room temperature and at all oven temperatures and made the surface even more dull. However, when acetone at 50 °C was used, it was observed that the surface was greatly improved in 3 and 5 min and in 15 min in the oven but staying in acetone for a long time (>5 min) damaged the material surface. For this reason, it was decided that the best parameters for surface improvement were kept in acetone at 50 °C for 3 min and then kept in the oven at 100 °C for 15 min, and it was decided to continue the characterization process with these parameters.

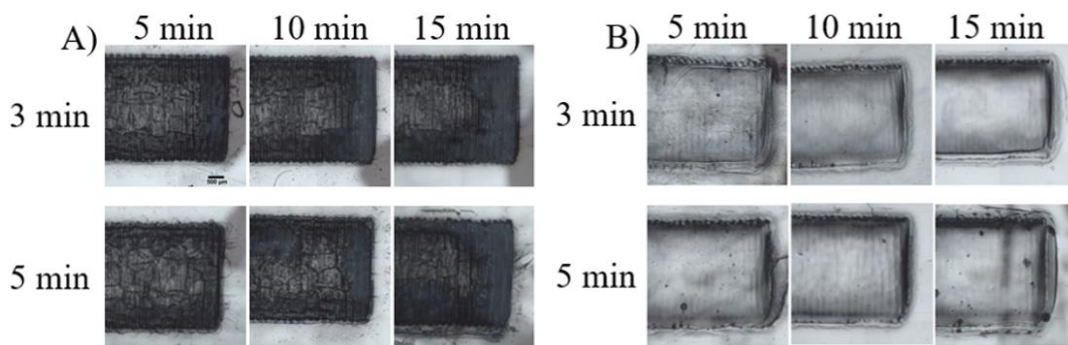


Figure 2.6. Effects of acetone temperature, time in acetone (3 and 5 min), and 100°C oven waiting time (5, 10, and 15 min) on surface healing. A) Acetone at room temperature (25°C). B) Acetone is close to its boiling temperature (50°C).

Later, to assess the effectiveness of the treatment procedure in enhancing optical clarity, open microfluidic channels on PMMA were compared under different conditions: untreated, subjected to heat treatment alone (at 100 °C for 15 min), treated with acetone alone (at 50 °C for 3 min), and treated with a combination of acetone and heat (Figure 2.7). It was observed that acetone initiated the dissolution and smoothing of PMMA. When combined with heat treatment, the PMMA became softened, facilitating the filling of grooves and reducing roughness caused by engraving. On the other hand, when only

heat treatment was applied, the porous structure started to decrease compared to untreated PMMA, but no significant effect on surface roughness was observed. In addition, although the surface roughness decreased significantly when only acetone treatment was applied, we observed that when it was not combined with heat treatment, there was no smooth surface equalization, especially at the channel edges. However, we have seen that when heat treatment and acetone treatment are applied together, they create a complementary effect and increase their effectiveness, making the channel surface smooth.

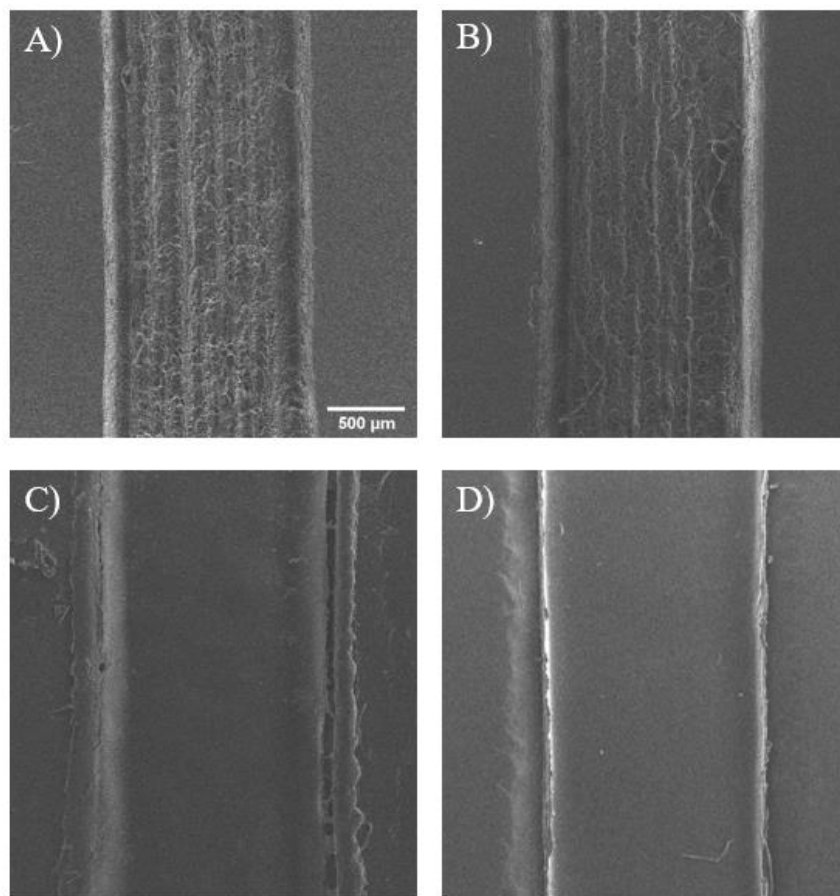


Figure 2.7. SEM of microfluidic channel surfaces engraved on PMMA. A) Untreated channel. B) Channel cured with heat at 100 °C for 15 min. C) Channel cured with acetone at 50 °C for 3 min. D) Channel treated with acetone at 50 °C for 3 min and then with heat at 100 °C for 15 min. Scale bars are 200 μm.

We further investigated the optical transmission properties of PMMA surfaces to observe the impact of surface roughness on optical transmittance (Figure 2.8). Bulk material surface, engraved-untreated surface, and treated surfaces were examined in 3 different color channels (red, green, and blue). As a result of our measurements, we saw that there was a significant increase and statistical difference ($p < 0.0001$) in the opacity of the untreated surface, decreasing approximately 3 times in all color channels compared to the bulk surface. However, it has been observed that the light transmittance of the treated surface in all color channels increased approximately 3 times compared to the untreated surface with statistical indifference ($p > 0.83$) and gained almost the same transparency as the bulk surface.

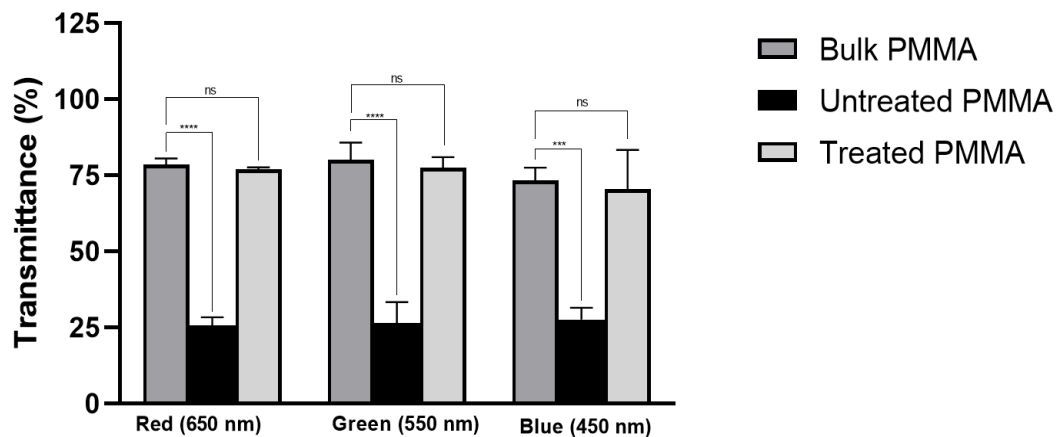


Figure 2.8. Light transmittance values of bulk, engraved, and engraved and then treated PMMA pieces for different wavelengths. ****, *** and ns indicate $p < 0.0001$, $p < 0.001$, and $p > 0.05$, respectively.

Moreover, contact angle measurements were conducted on PMMA surfaces to analyze the effect of our treatment methods on the material's surface hydrophobic features (Figure 2.9). When the bulk material surface and the engraved surface were compared, we observed that the hydrophobic property of the surface increased significantly due to the increase in surface roughness, with the contact angle increasing from $60.46^\circ \pm 1.62$ to $87.36^\circ \pm 0.31$ degrees. However, after the treatment was applied to the engraved surface, we observed that the angle decreased to $60.48^\circ \pm 2.17$ thanks to the

increase in the smoothness of the surface, and the surface properties showed statistical indifference ($p>0.99$) and regained similar properties with the bulk surface of the material.

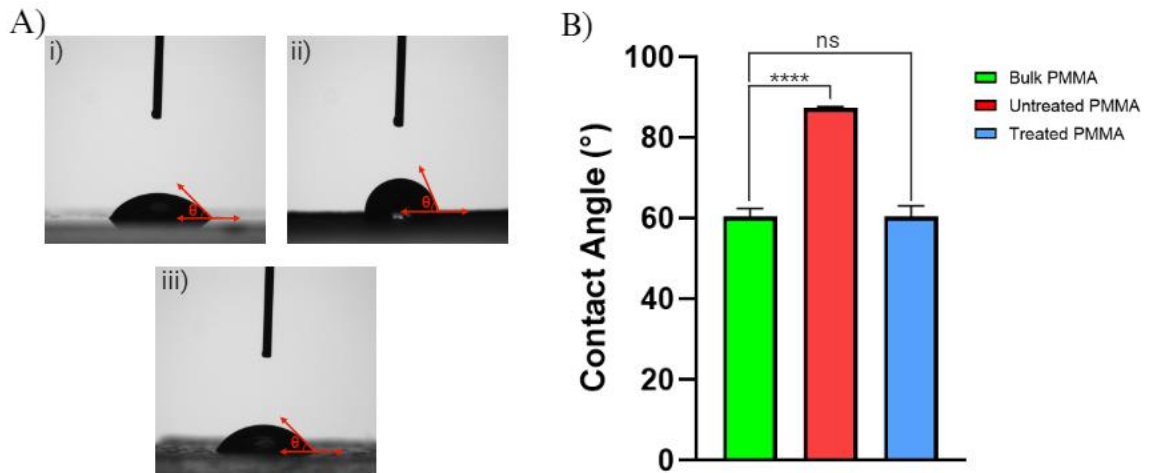


Figure 2.9. Contact angle measurement of the PMMA surfaces. A) Contact angle of the water droplet. i) Bulk PMMA surface, ii) Engraved PMMA surface and iii) engraved and then treated PMMA surface. B) Contact angle values for the bulk ($60.46^{\circ}\pm 1.62$), engraved ($87.36^{\circ}\pm 0.31$), and engraved and then treated PMMA ($60.48^{\circ}\pm 2.17$) surfaces. **** and ns indicate $p < 0.0001$, and $p > 0.05$, respectively.

2.5.2. Characterization of PMMA Bonding

Lap-shear test was performed to examine the bonding strength of PMMA pieces after treatments with acetone in different concentrations (50-100%) and heat at 100 °C in different durations (5-15 min) to observe the effect of the acetone concentration and curing time in the oven (Figure 2.10). We observed that there was no significant difference in bonding strength up to 70% acetone concentration, and an average bonding strength of 32.08, 32.23, and 31.30 MPa was obtained after 5, 10, and 15 min of heat treatment. We observed that when the concentration dropped below 70%, especially at 50% heat treatment in the oven for 5 min, the effectiveness of acetone decreased

significantly, and the bonding strength decreased by more than half to 12.81 MPa. However, even at low acetone concentrations (50% and 60%), we observed that the bonding strength increased again to 30.81 MPa and 33.17 MPa after 10 and 15 min of heat treatment. These results show that even at low acetone concentrations (<70%), we can achieve a bonding strength of more than 30 MPa when heat treated for 10 min or more, equivalent to the strength of PMMA itself (30.33 MPa).

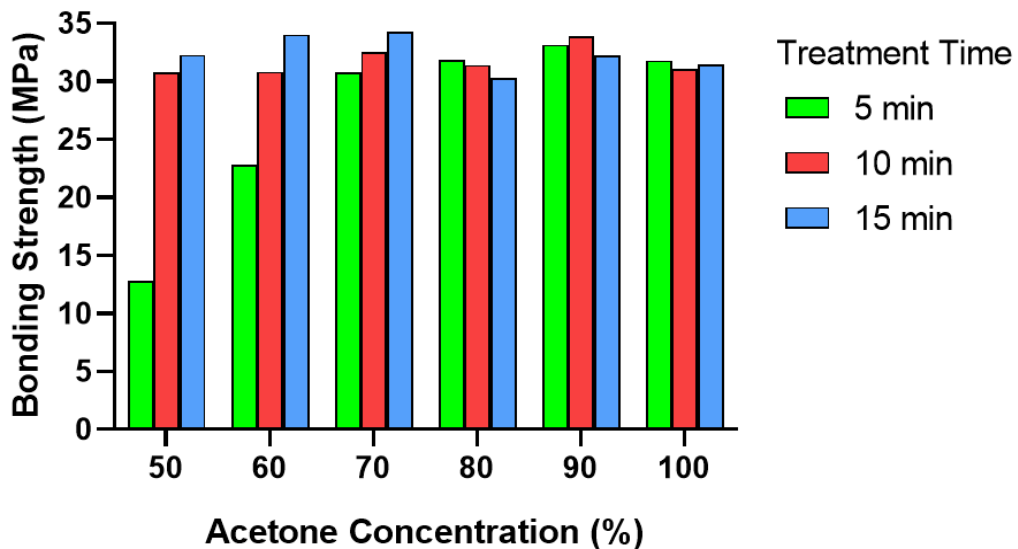


Figure 2.10. The effect of acetone concentration and temperature treatment time on bonding strength.

However, when we observed the bonding areas under the microscope, we observed that air bubbles could be trapped in the bonding area (Figure 2.11) which could lead to leakage problems during microfluidic channel fabrication. We decided that 5 min was sufficient for bonding time as the bonding process was fast and had approximately the same bonding strength as long as the acetone concentration was not low. In the examination, when the bubble ratio in the images is compared to the entire bonding area, we found that the use of pure acetone in the bonding process is most efficient when combined with a 5-minute heat treatment since the bubble formation in the bonding area when using pure acetone has a very low rate of 1.8% compared to other concentrations.

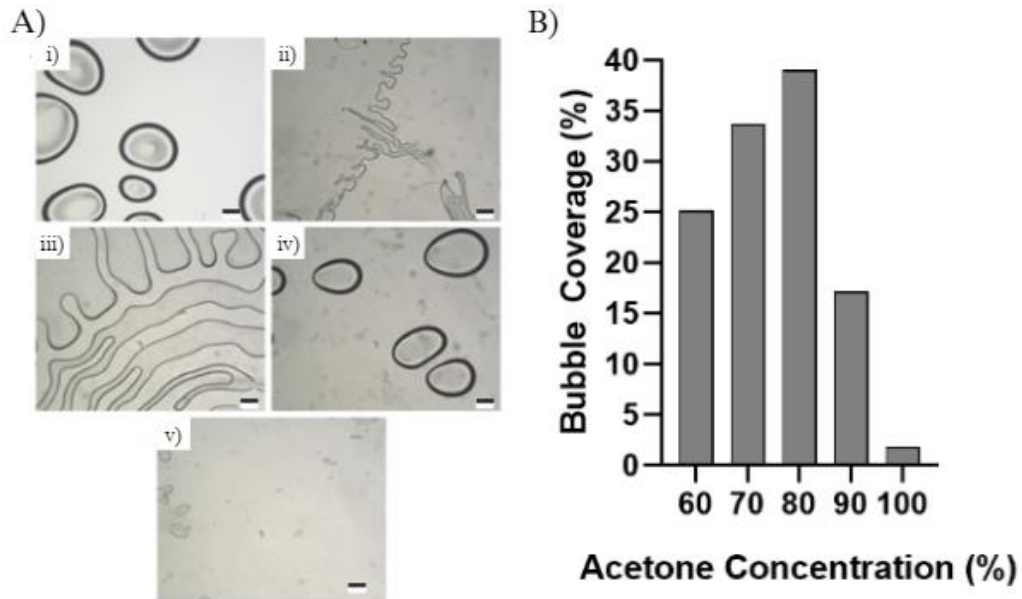


Figure 2.11. Bubble formation on the bonding surfaces after 5 min heat treatment at 100°C. A) Micrographs of bonding areas treated with different acetone concentrations: i) 60%, ii) 70%, iii) 80%, iv) 90% and v) 100%. Scale bars are 200 μm . B) Surface coverage of air bubbles on the bonded area.

2.5.3. Fabricated Monolithic Microfluidic Devices

In order to test the adaptability of the surface enhancement and bonding methods we developed and the feasibility of microfluidic chip fabrication, channels with a depth of 150 μm and dimensions of 1 x 20 mm (width x length) were engraved on a 2 mm thick PMMA sheet. The engraved channel surfaces were prepared as untreated, only heat treated at 100 °C, only acetone treated at 50 °C for 3 min, and acetone and heat treatment were applied together, and then they were combined with the bonding method we developed by combining channel engraved surfaces with a secondary PMMA. Cross-section images of the created monolithic microfluidics were analyzed under SEM (Figure 2.12). As a result of our observations, the channel depths are $99.28 \pm 4.15 \mu\text{m}$ in untreated channels, $116.120 \pm 4.09 \mu\text{m}$ in only heat-treated channels, $73.76 \mu\text{m}$ in only acetone-treated channels, and when both processes are combined, the channel dimensions are $145.12 \pm 3.21 \mu\text{m}$, and the channel widths are $1244.08 \mu\text{m}$, respectively. $\pm 17.54 \mu\text{m}$,

1264.16 ± 16.93 μm, 1123.7 ± 6.45 μm and 1097.45 ± 1.59 μm were observed. It was observed that when acetone and heat treatment were not applied together, the roughness on the channel surfaces caused the channel surface to adhere to the secondary PMMA, leading to blockage of the channels.

Additionally, it was observed that the bonding method did not cause any defects on the channel edges and did not harm the treated channel smoothness. The results showed us that the heat treatment had an effect of increasing the channel depth by softening the material and allowing it to spread, while the acetone treatment did not have an effect of increasing the channel depth because it etched the defects on the surface and did not fill the channel gaps. We also observed that the method we developed achieved the desired channel depth by applying these two processes together, filling the gaps on the channel surface and eliminating surface roughness.

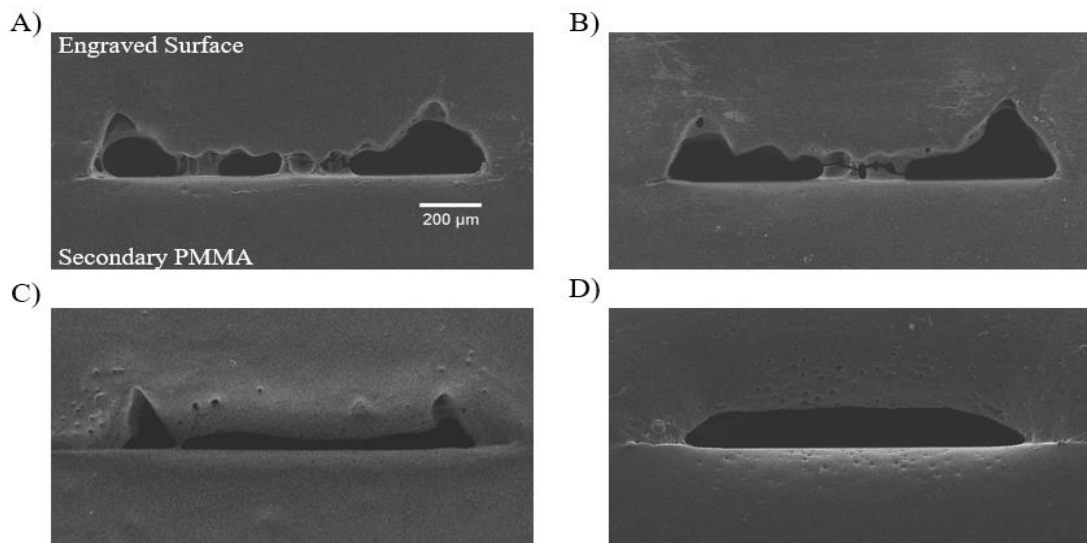


Figure 2.12. SEM of cross-section views of bonded channels. The images were taken from A) engraved, B) engraved and then treated with heat at 100 °C for 15 min, C) engraved and then treated with acetone at 50°C for 3 min and D) engraved and then treated with acetone at 50°C for 3 min and with heat at 100 °C for 15 min. Before bonding, open microfluidic channels were fabricated as explained and then bonded to a secondary flat PMMA piece.

After observing that our treatment and bonding methods could work together, we tested the smallest channel size we could create with our method. Thanks to our method, we managed to produce a channel with a width of 400 μm and a depth of 100 μm . Although the channel width was narrow and microfracture-like structures were formed at the edges of the channel due to laser heat, it was observed that there was no leakage in the channel after 24 hours of soaking in water (Figure 2.13).

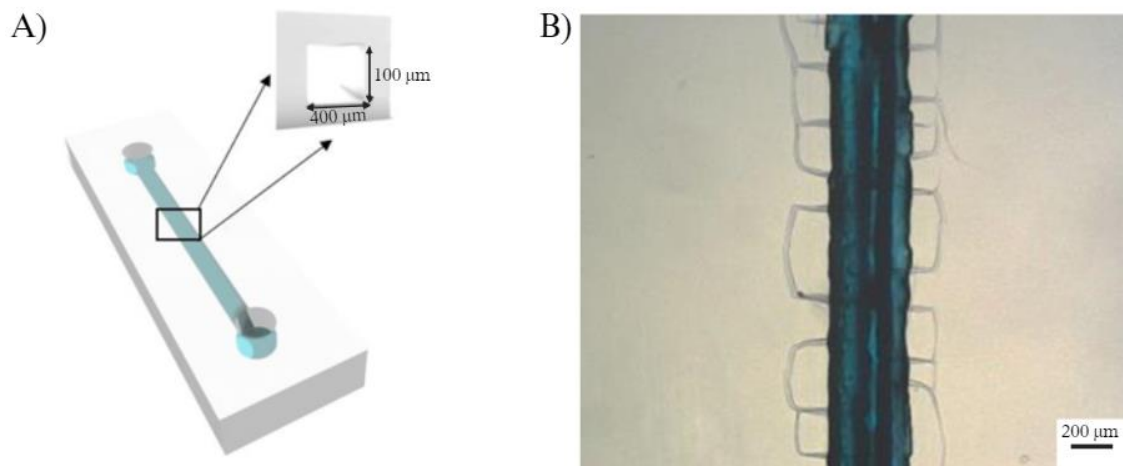


Figure 2.13. Microfluidic channel fabrication using the bonding method. A) Illustration and B) Micrograph of the microfluidic channel containing blue food dye solution. The scale bar is 200 μm .

We also examined whether the method we developed a leak-proof bonding by monitoring the liquid evaporation in the channel. For this purpose, colored liquid was injected into the channel with a liquid volume of 10 μL and monitored for 72 hours (Figure 2.14). To better observe the effect of bonding, chips were used in which both inlets were open, the inlets were closed with an additional 3rd PMMA layer with the help of clips, and the inlets were closed by bonding with the 3rd PMMA layer. While there was no liquid left in the chip with the inlets open after 24 hours, it was observed that there was no liquid left in the PMMA chip held with clips after 48 hours. However, in the third bonded chip, it was observed that even after 72 hours, the liquid in the channel was still

present and did not evaporate. This shows us that the method we developed can be an alternative to hermetic seal in the future by providing an air-tight seal.

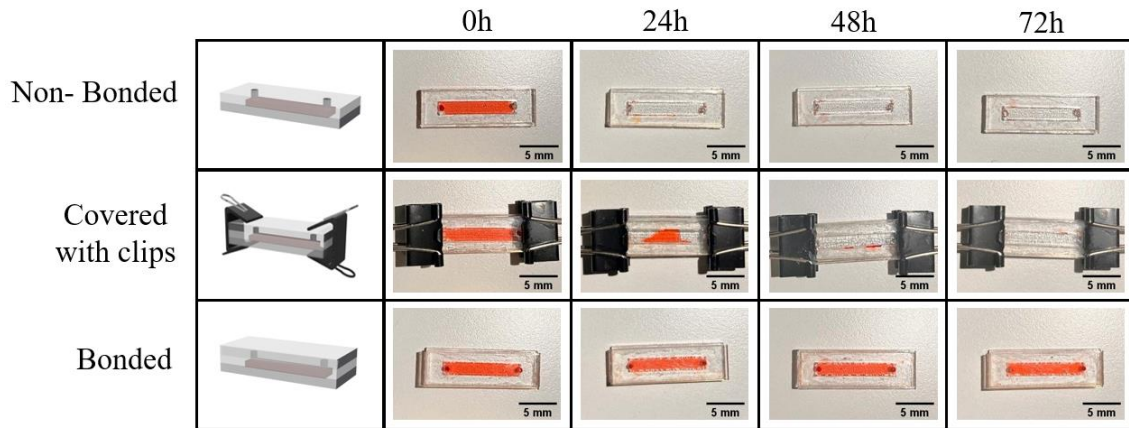


Figure 2.14. Time-lapse images capturing the evolution of microfluidic channels filled with a red food color solution over a 72-hour inspection period. The channels' inlets and outlets were sealed either by placing a PMMA piece over them, clamping the piece onto the chip, or bonding it to the chip.

2.6. Comparison with Different Treatment and Bonding Methods

Even though the developed methods have expanded and facilitated the use of PMMA in microfluidics fabrication, unfortunately, they still need to be improved (Table 2.1). After the surface enhancement process, a bonding strategy that is compatible and complementary to the surface enhancement needs to be developed.⁷³ In addition, bonding methods after surface enhancement are time-consuming and are not complementary to surface improvement, thus reducing the practicality of these methods.^{74,75} In addition, because of the bonding of engraved channels without any processing, the optical and surface properties that make PMMA an advantageous material are damaged.^{79,86} In addition, the bonding strengths obtained are not very high, making it difficult to adapt them to systems exposed to high forces, especially centrifugal microfluidics. In addition, although high bonding strength can be achieved in methods where channels are created

by cutting an extra PMMA layer, the channel height in these methods depends on the height of the PMMA (>0.5 mm).^{84,85}

Table 2.1. Comparison Between Several Surface Enhancement and Bonding Techniques for the Fabrication of PMMA-Based Microfluidics.

Ref.	Surface enhancement/ Bonding	Surface enhancer/ Bonding method	Optical Clarity	Surface enhancement time/ Bonding time	Bonding strength	Number of PMMA layers
(Z. K. Wang et al., 2011)	+/-	Acetone mixed with ethanol/-	+	10 min/-	-	1
(Matellan & del Río Hernández, 2018)	+/+	Acetone vapor/Epoxy resin	+	25 min/48 h	NR	2
(Ogilvie et al., 2010)	+/+	Chloroform vapor/Hot press	+	4 min/30 min	NR	2
(Faghih & Sharp, 2019)	-/+	- /Dichloromethane mixed with IPA	+*	-/15 min	4.2 MPa	3
(Madadi et al., 2023)	-/+	-/Ethanol and IPA	+*	-/40 min	3.48 MPa for ethanol and 6.21 MPa for IPA	3
(Bamshad et al., 2016)	-/+	-/IPA	-	-/50 min	28.47 MPa	2
(Trinh et al., 2020)	-+	-/Acetic acid	-	-/20 min	13.7 MPa	2
Our Method	+/+	Pure acetone/ Pure acetone	+	3 min/15 min	>30 MPa	2
<p><i>NR: Not Reported</i> <i>* No surface enhancement is needed, since an additional PMMA layer was fully cut to form the channel.</i></p>						

2.7. Conclusion

In this chapter, a fast, easy, durable, and low-cost fabrication technique is developed for PMMA-based microfluidics by utilizing pure acetone as both surface enhancement and bonding agent. PMMA holds great importance for microfluidic fabrication due to its beneficial features such as transparency, low autofluorescence, and biocompatible. However, creating micro channels on PMMA is not always simple. For many techniques, channels are engraved on the PMMA surface using a laser cutter. During this process, due to the heat from the laser cutter, surface roughness and defects increase drastically. This defect decreases the transparency and also disturbs the laminar flow inside the channel. To maintain smooth and transparent channels, different chemicals and vapors are applied to the PMMA surface. However, these chemicals can be highly toxic, and steps can be time-consuming. In addition, creating high-strength quality bonding holds great importance to create PMMA-based microfluidics. The presented research offers a simple and single solvent method that can both enhance surface quality and maintain high-strength bonding. In this research, combining hot acetone treatment with heat treatment, the engraved channel surface self-heals itself and gains its bulk state surface features (transparency, smoothness, and hydrophobicity). Also in this work, using the same solvent as a bonding agent, a bonding strength greater than the PMMA's tensile strength and an airtight seal can be achieved. With this method, a channel with a height of 150 μm can be produced. Thanks to this method, we can fabricate a high-bonding strength PMMA-based microfluidic chip using a single solvent (pure acetone) without any complex steps and low cost that can be used for both microfluidics and centrifugal microfluidics. We anticipate that our technique will be used in various biomedical applications in the future.

CHAPTER 3

ISOLATION AND ENRICHMENT OF EXOSOMES WITH CENTRIFUGAL MICROFLUIDIC DEVICE

3.1. Introduction

Particles with sizes of 150 nm and below are called nanoparticles.⁹⁵ Due to the size of these particles, they gain unique physical and chemical properties that differ from their bulk states in macro sizes.⁹⁶ Nanoparticles can be classified into two groups, depending on whether they are found in nature or not (such as exosomes, viruses found in nature) and hard (such as inorganically synthesized gold and silver nanoparticles).⁹⁷ Owing to the unique properties of these particles, they are widely used in many different fields such as electronics, cosmetics, health, and pharmaceutical industries.⁹⁸

In this chapter, exosomes were collected from the cell medium within 1 hour without the need for any marker. Exosomes could be collected from the bottom of the channel as a result of centrifuging the exosome sample loaded into a channel half-filled with PBS for 60 min at 9000 rpm. With this study, it was possible to isolate exosomes quickly, cheaply, and simply and increase their concentration. We expect that in the future, by testing different body fluids, the use of exosomes as biomarkers in IVDs will become widespread.

3.2. State-of-the-Art of Exosome Isolation

Extracellular vesicles (EVs), which belong to the soft nanoparticle class, are membrane-bound structures and most of them are secreted by cells.⁹⁹ These vesicles serve

as intracellular cargo thanks to structures such as protein, RNA and DNA.¹⁰⁰ EVs have different nomenclature and classification depending on size, density, morphology, lipid composition, and protein composition.¹⁰¹

Compared to other EVs, exosomes are distinguished by their unique intracellular biogenesis.¹⁰² Exosomes, whose sizes vary between 30-150 nm, are bowl-like structures that appear under the transmission electron microscope (Figure 3.1).¹⁰³ Exosomes can be found in almost all biological samples (saliva, blood, urine, etc.).¹⁰⁴ Because they serve as intracellular cargo, they have great potential to be used as biomarkers for disease and toxicity.¹⁰⁵ Exosomes vary in composition because they can be secreted from many cell types.¹⁰⁶

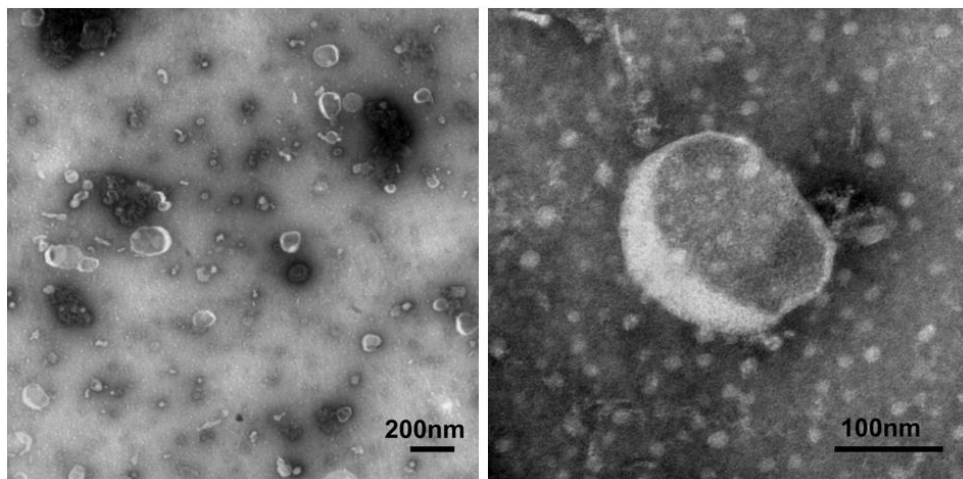


Figure 3.1. TEM images of the exosomes (Source: Lin et al., 2021).

Depending on their varying sizes, exosomes serve various biological functions.¹⁰⁸ However, the complex structure of cell debris and biological fluids within the sample can affect the analysis of exosomes.¹⁰⁹ Therefore, impurities present in the sample can also affect the molecular profile of exosomes, including proteomic and transcriptomic analyses. This may lead to false positive or negative results when exosomes are used as biomarkers, thus impairing the biomarker potential of exosomes.¹¹⁰

When developing EVs analysis and isolation techniques for drug delivery applications, large quantity of exosomes with enhanced purity and specificity should be

considered.¹¹¹ Since the structures (DNA, RNA) found within exosomes can provide prognostic information for various diseases, these methods should guarantee that the exosomes' composition, biological activity, and structure remain unaltered.¹¹² Intact exosomes can be infused with medications and aid in their transport their uptake by recipient cells.¹¹³

3.2.1. Conventional Methods for Exosome Isolation

To ensure the homogeneity of nanoparticles/exosomes, there are two complementary steps which are isolation and enrichment.¹¹⁴ In the isolation stage, nanoparticles of desired sizes are isolated.¹¹⁵ However, the concentration of nanoparticles may decrease during this process.¹¹⁶ For this reason, enrichment processes that increase the concentration are needed after isolation.⁹⁷

There are standardized methods such as ultracentrifugation, electrophoresis, chromatography, and filtration, which are also used in nanoparticles, for the isolation and enrichment of exosomes.¹¹⁷ These methods can basically be divided into three different classes; separation via an external field, elimination, and colloidal stability.¹¹⁸

3.2.1.1. Separation via External Field

The method of separation using an external field is based on distinguishing the characteristic properties of nanoparticles such as size, density, and electrical or magnetic behavior.¹¹⁹ Today, ultracentrifugation and gel electrophoresis are the most commonly used methods to separate and collect nanoparticles.^{120,121}

Ultracentrifugation works on the principle of ensuring the accumulation of particles of the same density by centrifugal force and is an ideal technique for classifying nanoparticles according to their size and shape and is the most widely used technique for purification of exosomes today.¹²¹ Even though this method is easily applicable, the need

for an ultracentrifuge device and expensive materials restricts the widespread use of this method.¹²²

Gel electrophoresis is widely used to obtain good quality purified genomes and nanoparticles and is a technique based on electrical force rather than mechanical force.¹²⁰ Although it is a useful technique for genomics and proteomics research, many processing steps are required, which prolongs the purification time.¹¹⁸

3.2.1.2. Sieving Method

The sieving method is another nanoparticle separation method that includes chromatography and nanofiltration techniques.¹²³ Chromatography is based on the use of two phases (fixed and mobile) and the separation of the sample according to fraction ratios while in the mobile phase.¹²⁴ Although it is a highly efficient method, it requires long processing times, multiple steps, and special materials for each sample.¹²⁵

Nanofiltration is a basic technique based on filtering particles according to their size. With this method, it is possible to process large sample volumes quickly.¹²⁶ However, separation efficiency may decrease due to clogging of nano filters.¹²⁷

3.2.1.3. Colloidal Stability

Colloidal stability is used to separate nanoparticles by changing their stability and diffusion. For this purpose, size-selective precipitation (SSP) or solvent addition can be done¹²⁸ SSP is used to change the nanoparticle structure by aggregating them. After precipitation, samples are centrifuged, and non-precipitation is based on isolating particles.¹²⁹ However, this method also has time-consuming and complex steps.

The above-mentioned techniques require requirements such as high sample volume and multi-step preparation, which seriously limits the use of these methods. In addition, each separation method needs precise optimization processes for the separation of different sized nanoparticles based on sample features (density, purity, solubility

etc.).¹³⁰ In addition, these methods are time-consuming and costly.¹³¹ Therefore, new methods are needed for fast, cost-effective, and easy exosome purification.

3.3. Microfluidic Technologies for Exosome Isolation

Due to the size of microfluidics, it requires a small sample volume, prevents sample loss during operations, and provides cost-effective analysis.¹³² For this reason, there are studies on exosome isolation using microfluidic technology. Studies on exosome isolation have been conducted using immunoaffinity, acoustics, and filtration in microfluidics.¹³³ For example, an exosome isolation and detection method based on a microfluidic device that performs microsphere-mediated dielectrophoresis isolation and immunoaffinity detection has been developed.¹³⁴ With this method, 1.4×10^3 to 1.4×10^8 exosomes per mL could be obtained with a detection limit of 193 exosomes per 1 mL. In another study, a device called ExoChip was designed to separate CD63-specific exosomes from serum.¹¹⁴ The surface of the designed microfluidic platform was coated with CD63 antibodies. Thanks to the developed system, isolation of exosomes could be achieved within 1 hour.

3.3.1. Centrifugal Microfluidics for Exosome Isolation

There are studies in which centrifuge-based microfluidics, a branch of microfluidic systems, are used for exosome separation and enrichment (Figure 3.2).

Inside a centrifugal microfluidic system, Centrifugal, Coriolis, and Euler forces, also called pseudo forces, occur due to rotation and constitute the dominant forces in the centrifugal microfluidic system (Figure 3.3).¹³⁷

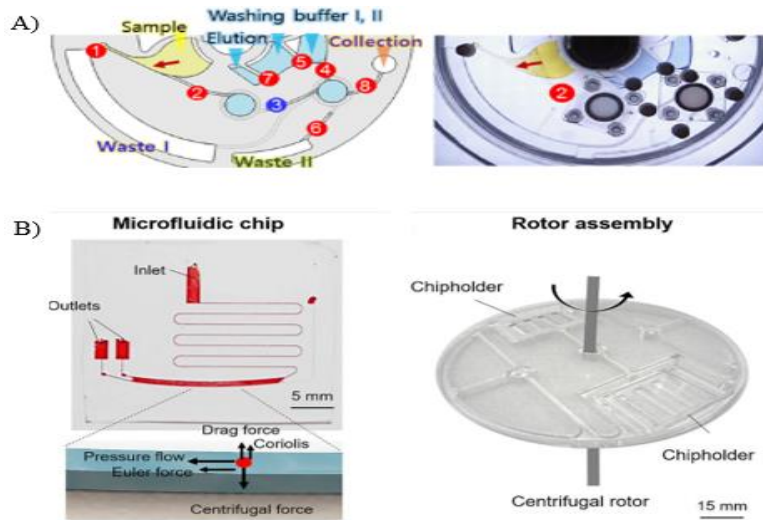


Figure 3.2. Centrifugal microfluidic devices for exosome isolation. A) Nano filter-based exosome isolation (Source: Yeo et al., 2018). B) Micro hydrodynamic based exosome isolation (Source: Woo et al., 2017).

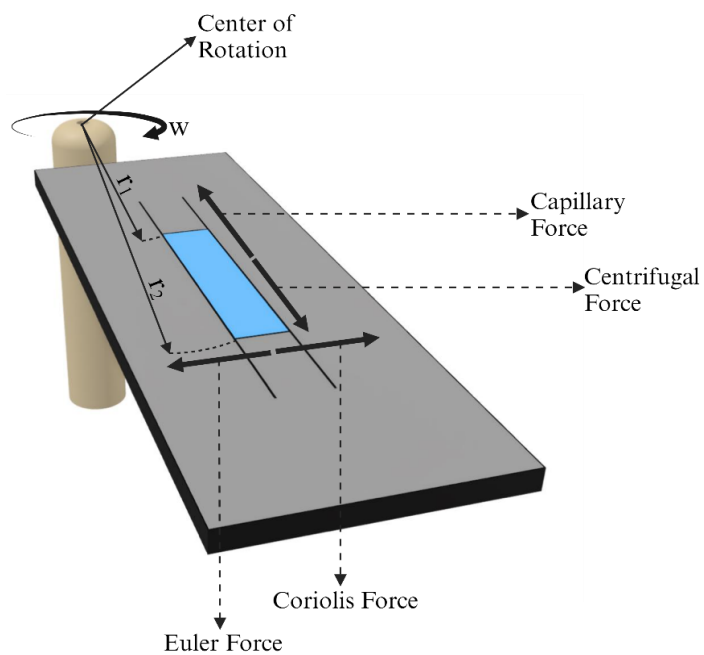


Figure 3.3. Illustration of the acting forces on a centrifugal microfluidic.

The centrifugal force (f_{cf}), which is always directed outward from the platform center, creates a centripetal acceleration in the same direction.¹³⁸ In Equation 3.1, m refers to the mass of the liquid in the chip, r is the distance of the chip from the platform center, and w is the angular velocity.

$$f_{cf} = mw^2r \quad (3.1)$$

Since the liquid inside the chip cannot be compressed and the head and end of the liquid are at different distances (r_1 and r_2) from the platform center, the pressure on the liquid (p_{cf}) causes the liquid (ρ_l) to move outward from the center (Equation 3.2).³³

$$p_{cf} = \int_{r_1}^{r_2} \rho_l w^2 r dr = \frac{1}{2} \rho_l w^2 (r_2^2 - r_1^2) \quad (3.2)$$

In addition to the centrifugal force, two different forces are effective: Coriolis (f_{co}), which originates from the rotation of the chip and occurs in the opposite direction to the direction of rotation, and perpendicular to the course of liquid flow, and Euler (f_e), in the same course as the course of rotation and perpendicular to the direction of liquid flow (Equation 3.3 and 3.4).^{33,139}

$$f_{co} = -2mw \times v = -2mw \times drdt \quad (3.3)$$

$$(3.4)$$

$$f_e = -m \frac{dw}{dt} \times r$$

The Coriolis force is a speed-dependent force and occurs if the acceleration due to rotation is not equal to 0.¹⁴⁰ Non-pseudo internal forces such as viscosity and capillary effect, which are not pseudo forces, also play important roles in fluid manipulation.¹⁴¹ To transport high-viscosity liquids, a higher force must be applied compared to low viscosity

liquids.¹⁴² In addition, if the channel width is not fixed and has a variable structure, it should be taken into consideration that the capillary force opposite to the flow direction of the liquid will be different in the channel.¹⁴³ Because of these phenomena, the centrifugal force can be easily adjusted by changing the angular velocity.¹⁴⁴ In addition, liquid flow can be achieved by keeping the centrifugal force greater than the capillary force and other forces, while liquid flow can be stopped by keeping it minimum.

For example, a fast, label-free, and precise method for EV isolation and quantification has been developed using a microfluidic integrated with two nano filters (Exodisc).¹³⁵ Preliminary from simple biological specimens, examples include cell culture supernatant or urine from cancer patients, which can be used for the automated enrichment of EVs. size of 20–600 nm was accomplished within 30 min using a benchtop-sized centrifugal microfluidic device. In a different study, the isolation and extraction of nanoparticles were performed in a single chip.¹³⁶ The developed system was able to achieve 90% isolation and 85% purity extraction of nanoparticles.

3.4. Materials and Methods

3.4.1. Fabrication of Falcon Tubes Compatible with Bench-Top Centrifuge

In order for centrifugal microfluidic chips to work in harmony with bench-top centrifuge devices found in almost every laboratory and to avoid the need for an external centrifuge system, falcon tubes compatible with the rotor, which takes 6 falcon tubes of 50 mL at 45°, were designed with a computer-aided drawing program (Shapr3D, Hungary) and then produced with a 3D printer (Ultimaker 2+ Connect, Netherlands) (Figure 3.4).

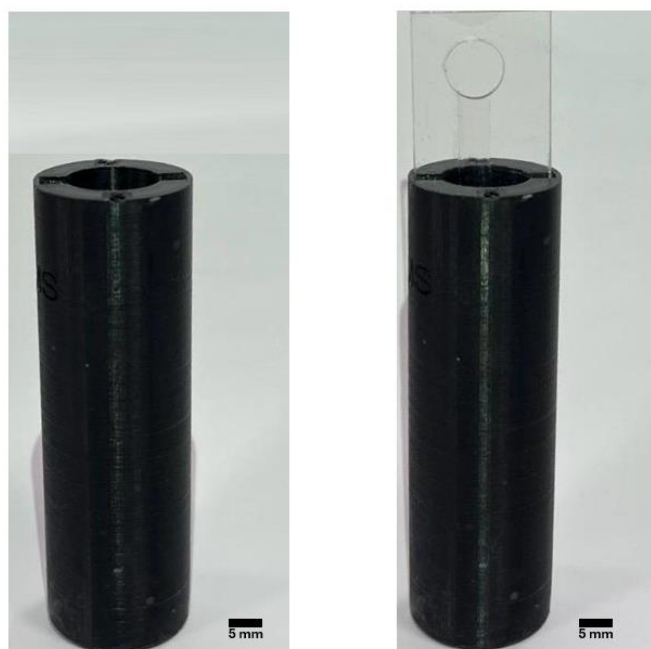


Figure 3.4. Image of the 3D printed falcon tubes that is compatible with bench-top centrifuge device.

3.4.2. Fabrication of Microfluidic Chip for Nanoparticle Isolation and Collection

A microfluidic chip design with a 60 μL dead-end channel was used in the determination of the isolation of nanoparticles and exosomes protocol. 5x50 mm (width \times length) channels with a depth of 200 μm were engraved on the surface of 25x75 mm (width \times length) PMMA (Akpolimer, Turkey) with a thickness of 1 mm using a laser cutter equipped with a 40W CO_2 laser (Figure 3.5A) (Makeblock LaserBox, China). The engraved chips were subjected to the surface improvement and bonding processes developed in Chapter 2, and dead-end microfluidic chip fabrication was completed.

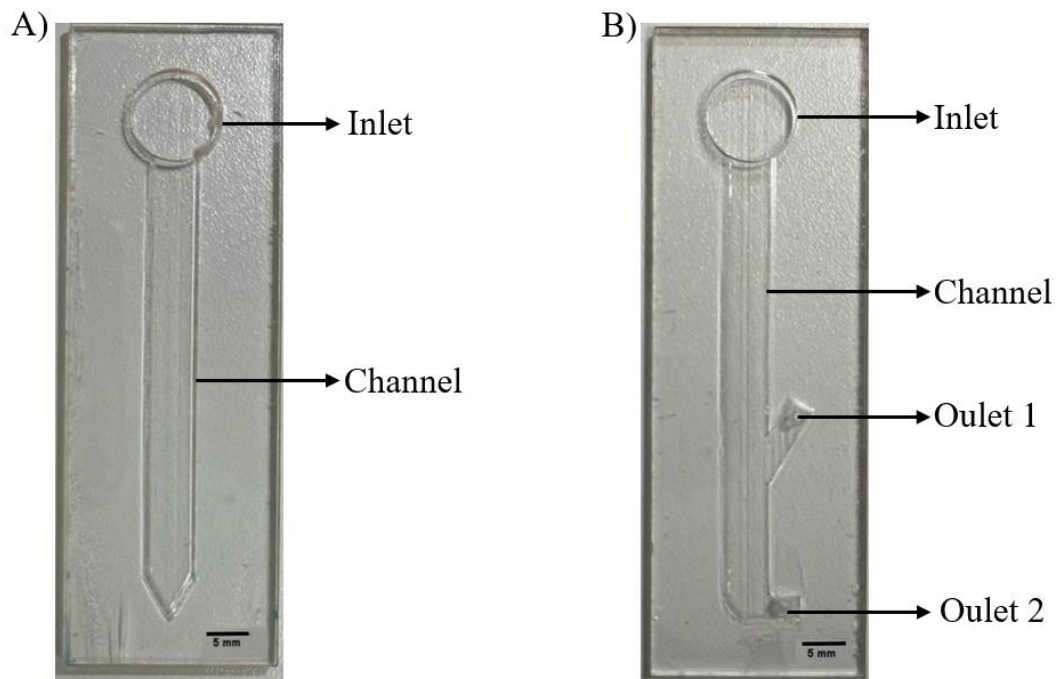


Figure 3.5. Microfluidic chips used in nanoparticle and exosome isolation. A) Microfluidic chip where the isolation protocol is carried out. B) Chip design in which isolated nanoparticles and exosomes can be collected. Outlet 1 is for the collection of the top liquid. Outlet 2 is for the collection of isolated particles.

In order to collect the isolated nanoparticles and exosomes, a chip design with two collection outlets was used, allowing a 60 μL dead-end channel to be collected, increasing the channel volume to 50 μL (upper part of the channel) and 10 μL (bottom part of the channel) (Figure 3.5B). The outlets were thinned on the PMMA surface during laser cutting by adjusting the cutting speed to 90 $\text{mm}\cdot\text{s}^{-1}$ and the laser beam power to 40W (100%). After isolation, the upper outlet, which was thinned first, was broken and 50 μL volume of the channel was collected. Then, the lower outlet was broken and the remaining 10 μL was collected and the particles were collected for analysis.

3.4.3. Characterization and Collection of Nanoparticles

For the characterization of nanoparticles, fluorescence-labeled (green, red, orange) polystyrene particles with sizes of 50, 100, and 200 nm were used (Lab261, USA) for adaptability with exosomes. All particles were used by diluting 1:100 in PBS (Gibco, UK) containing 0.1% Pluronic (Sigma, USA). Previously, the filling profiles of dead-end channels of different sizes depending on centrifuge speed and duration were examined by our team.¹⁴⁵ In this manner, before the nanoparticles were loaded onto the chips, the inside of the channel was incubated with 5% BSA (Sigma, USA) for 30 min to prevent nonspecific bonding within the channel.

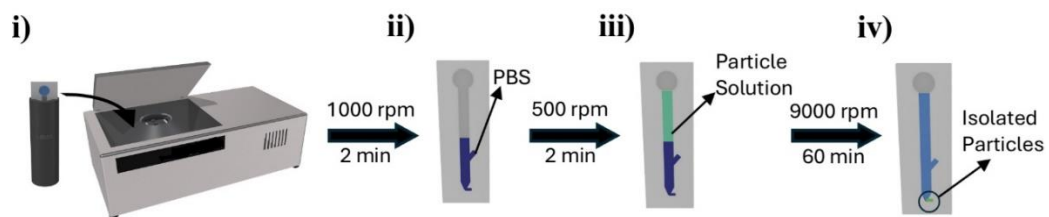


Figure 3.6. Isolation and the enrichment protocol for the nanoparticles. (i) After PBS is loaded into the inlet of the chip, the chip is placed in a falcon tube compatible with the centrifuge device and placed in the centrifuge device. (ii) Half of the channel volume is filled by centrifuging the chip at 1000 rpm for 2 minutes. (iii) Particle solution is loaded into the inlet part of the chip and centrifuged at 500 rpm for 2 minutes to fill the remaining volume of the channel. (iv) After the chip is centrifuged at 9000 rpm for 60 minutes, the particles are collected at the bottom of the channel.

Then, half of the channel volume (30 μ L) was filled by centrifugation at 1000 rpm for 2 min. The remaining volume (30 μ L) was filled with nanoparticles by centrifugation at 500 rpm for 2 min, and chip images were examined under a Zeiss M2N upright incubator microscope (ZEISS, Switzerland). The behavior of the particles in the

channel was centrifuged at 9000 rpm for 60 min and examined again under the microscope (Figure 3.6).

Channel images were divided into 8 zones and fluorescence intensities were measured (Figure 3.7). After the isolation protocol of the nanoparticles was determined, the particles at the top and bottom of the channel were collected.

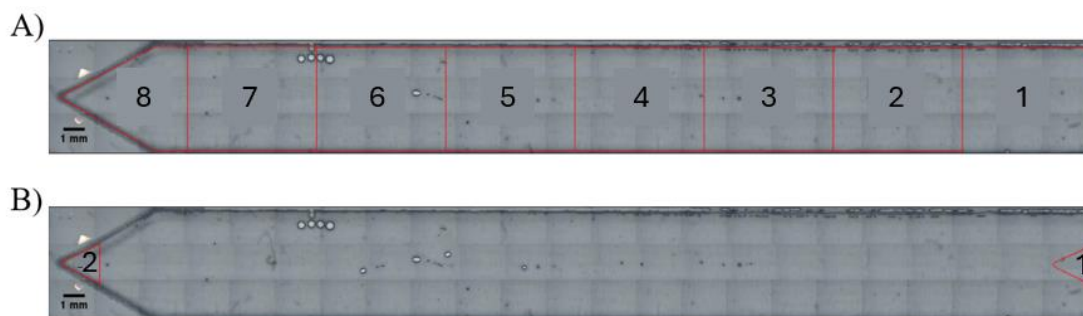


Figure 3.7. Microscope images showing analysis zones. A) Regions used for 8 zone analysis. B) Analysis regions used for top and bottom of the channel.

After the particles were collected at the bottom of the channel, the upper liquid (50 μL) was collected with the help of a pipette after breaking the number one outlet. Then, outlet number two was broken and the remaining liquid (10 μL) containing the particles collected at the bottom of the channel was collected (Figure 3.8).

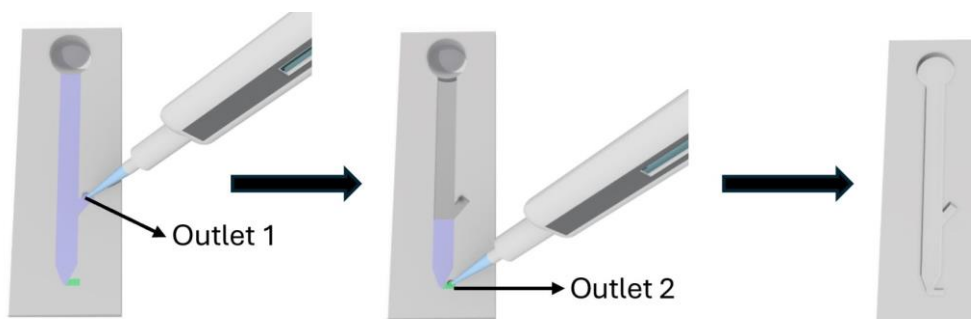


Figure 3.8. Collection protocol of isolated particles.

3.4.4. Preparation of Isolated Exosomes

The CD63-GFP MDA-MB-231 cell lines are cultured in 6 cm petri dish at 37 °C, 5% CO₂ with 60% confluency for 3 days in 5 mL Dulbecco's Modified Eagle Medium (DMEM 1X, Gibco, UK) with 10% FBS, 1% Penicillin/Streptomycin. After that point, the medium of cells is collected and used with ExoQuick ULTRA EV Isolation System (System Biosciences, USA, Cat #EQUltra-20TC-1, Lot # 231128-002). At the end of the kit isolation, the CD-63 GFP labeled MDA-MB-231 cell exosomes are isolated as 400 µL and storage at +4 °C for short term (up to 48 h) and storage at -80 °C for long term.

3.4.5. Preparation of Conditioned Medium Exosomes

Firstly, MDA-MB-231 is cultured in a 6 cm petri dish for 80% confluency. These cells are resuspended by Trypsin C (0.05% Trypsin, 0.02% EDTA) with incubation 5 min at 37 C, 5% CO₂. After that, the resuspended cells are centrifuged to solve them in 1 mL Dulbecco's Modified Eagle Medium (DMEM 1X, Gibco, UK) with 10% FBS, 1% Penicillin/Streptomycin. The 4×10⁵ cells are transferred to a new tube and DMEM is added to fill up to 2 ml. The prepared tube is spread to the 6-well plate and incubated at 37C, 5% CO₂ for 24h. These cells stick on the surface of a 6-well plate thus the medium is replaced by Serum Free DMEM with only 1% Penicillin/Streptomycin for 1 ml. Then the 48-h incubation is applied to accumulate exosomes in suspension. Lastly, the 1 mL medium is collected and applied to a centrifuge for 13.300 rpm-15 min, the supernatant of the solution is labeled as Conditioned medium (Figure 3.9).

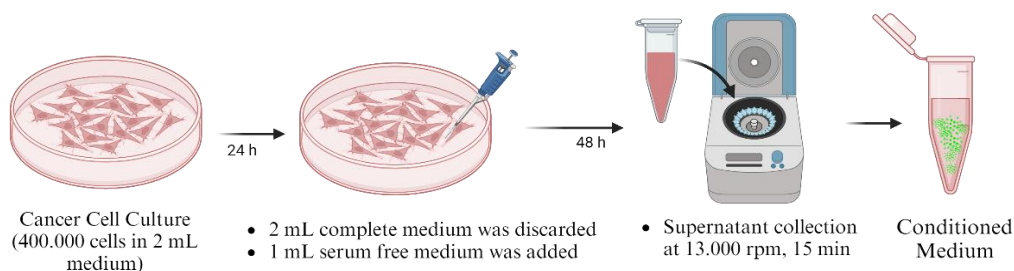


Figure 3.9. Collection protocol of the conditioned medium exosomes.

3.5. Statistical Analysis

Data were presented as the mean \pm standard deviation (SD) of at least three replications of studies. ImageJ was used to analyze microscope images. Two-way ANOVA combined with Tukey's multiple comparison test and hill slope was used to statistically analyze the data. These analyses were carried out using GraphPad software (Prism 8 version, GraphPad, USA).

3.6. Results

3.6.1. Movement of Nanoparticles in the Channel Depending on Time

In order to observe the time-dependent movements of polystyrene particles of varied sizes (50-200 nm) at 9000 rpm, particles were centrifuged for 60 min with 5-minute intervals and images were taken under a fluorescence microscope. First, half of the volume of the channel (30 μ L) was filled with PBS containing 0.1% Pluronic by centrifugation at 1000 rpm for 2 min, and the remaining volume (30 μ L) was filled with nanoparticles with varied sizes at 500 rpm for 2 min. It was observed that 200 nm particles started to accumulate after the 5th minute (Figure 3.10), 100 nm particles started to collect

at the end of 10 min (Figure 3.11) and 50 nm particles started to collect at the bottom of the channel, especially after at the end of 15 min (Figure 3.12).

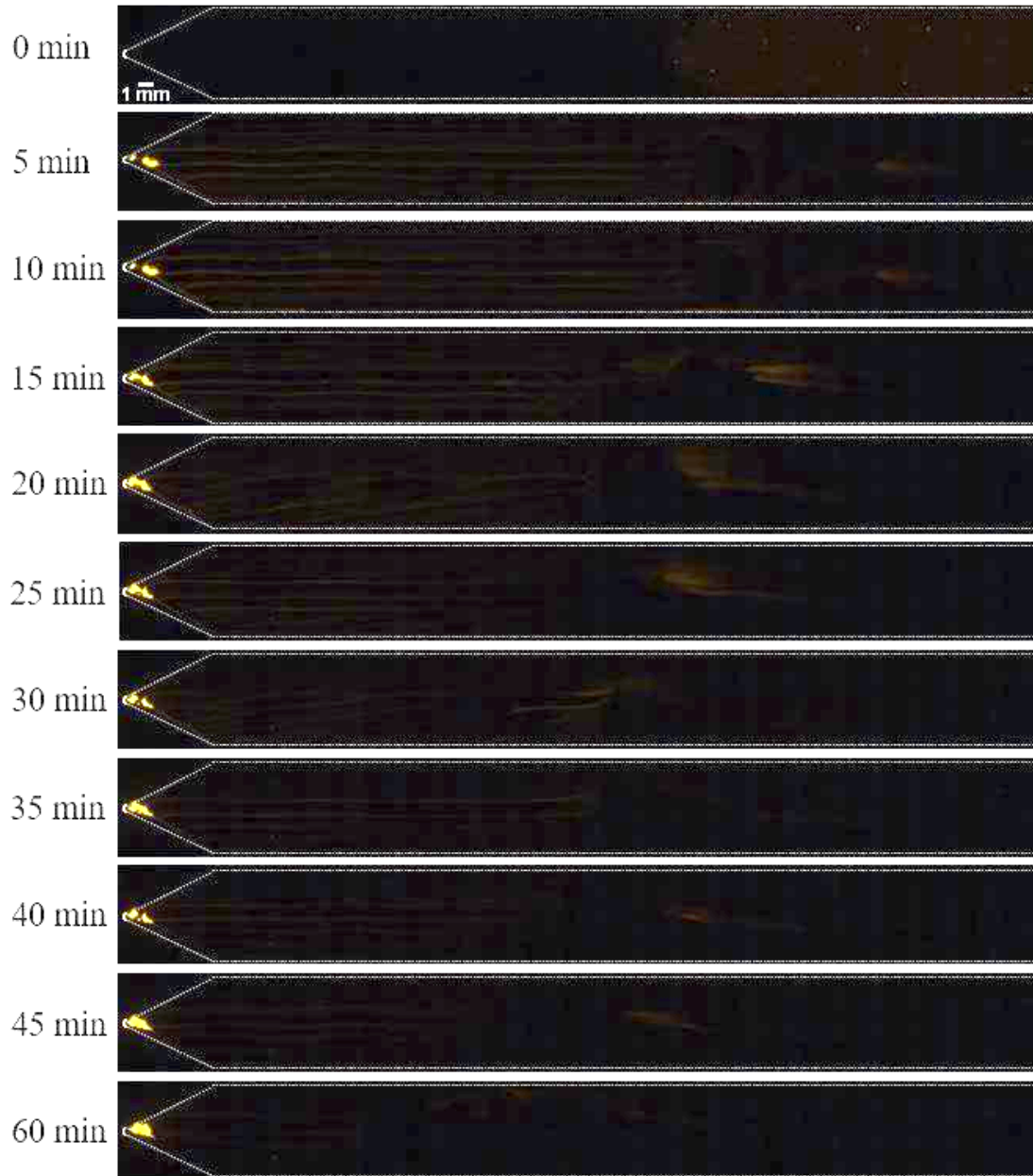


Figure 3.10. Microscope image of 200 nm particles aggregating in the time-dependent channel at 9000 rpm.

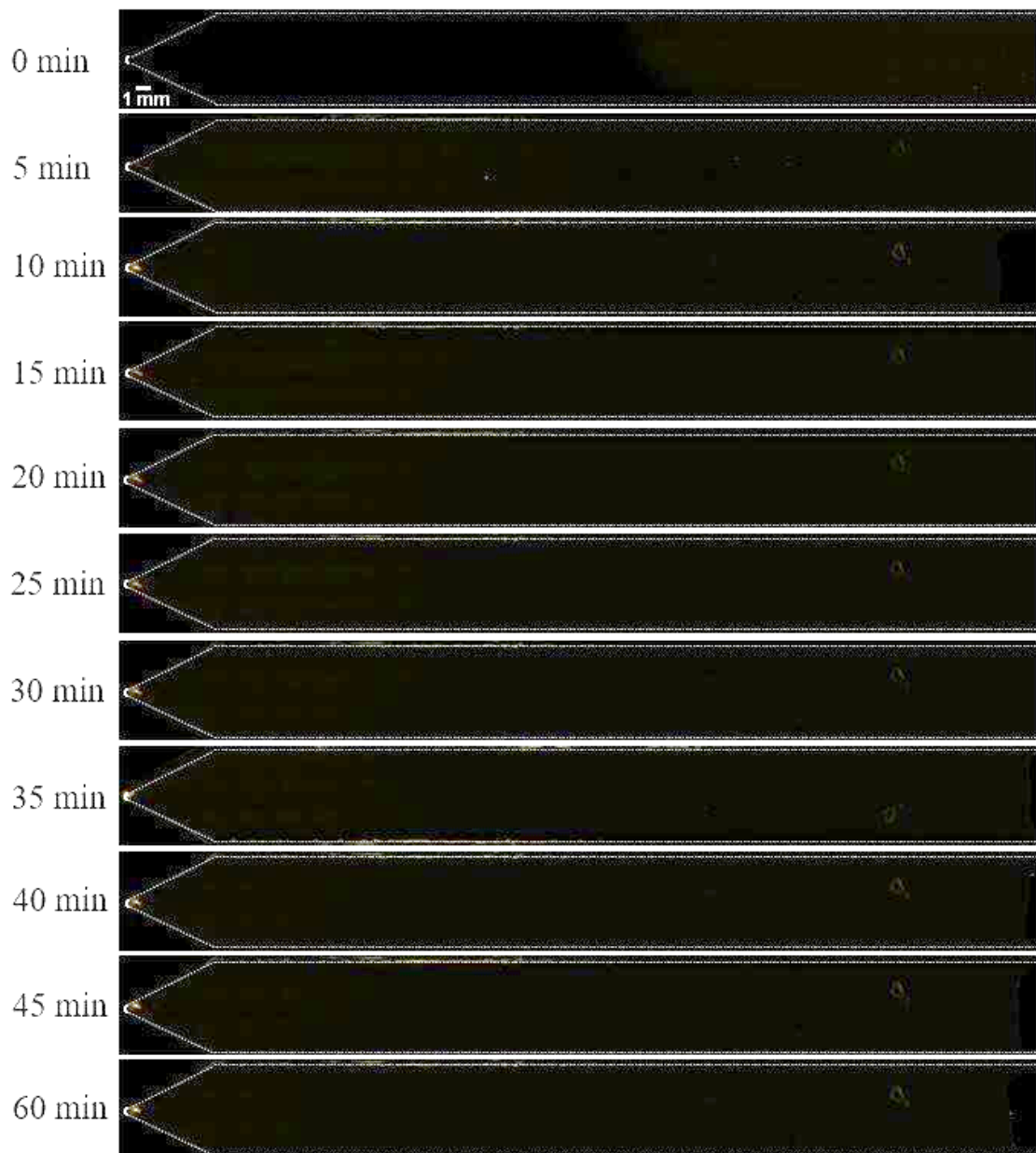


Figure 3.11. Microscope image of 100 nm particles aggregating in the time-dependent channel at 9000 rpm.

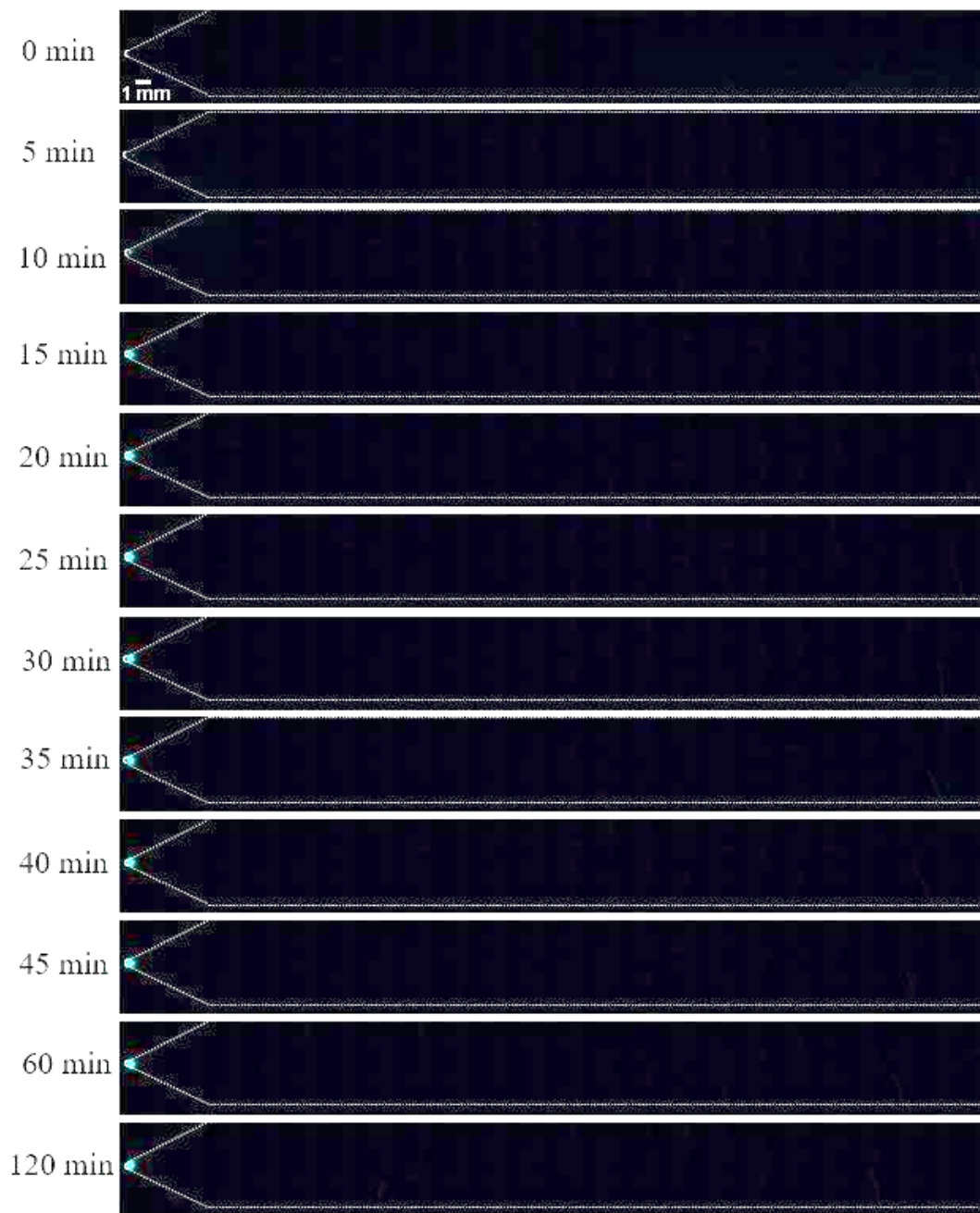


Figure 3.12. Microscope image of 50 nm particles aggregating in the time-dependent channel at 9000 rpm.

To observe that the radiation occurring at the bottom of the channel is nanoparticle and not a noise originating from PBS, it was observed whether PBS containing 0.1% Pluronic, used to dilute the particles, created noise under the microscope. For this, 60 μL of PBS was centrifuged at 1000 rpm for 2 min and then imaged under a fluorescence

microscope under different wavelengths of radiation. Then, the PBS-filled chips were centrifuged at 9000 rpm for 60 min and examined under the microscope again (Figure 3.13).

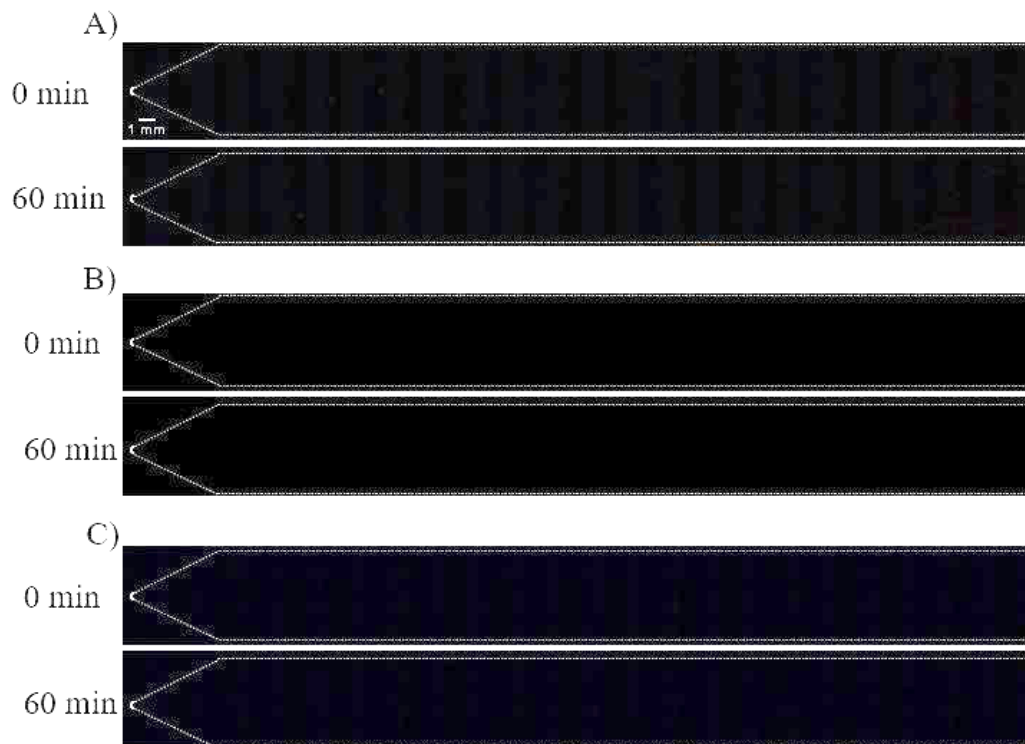


Figure 3.13. Before and after centrifuging PBS used as control for 60 min at 9000 rpm.

A) Images taken at the microscope image settings used for 200 nm particles.

B) Images taken at the microscope image settings used for 100 nm particles.

C) Images taken at the microscope image settings used for 50 nm particles.

No radiation was observed before and after for 3 different wavelengths (green, red, orange). In addition, these images and channels were divided into 8 equal zones and mean intensity values were measured. It was observed that there was no statistical difference ($p > 0.97$) between the zones before and after centrifugation (Figure 3.14).

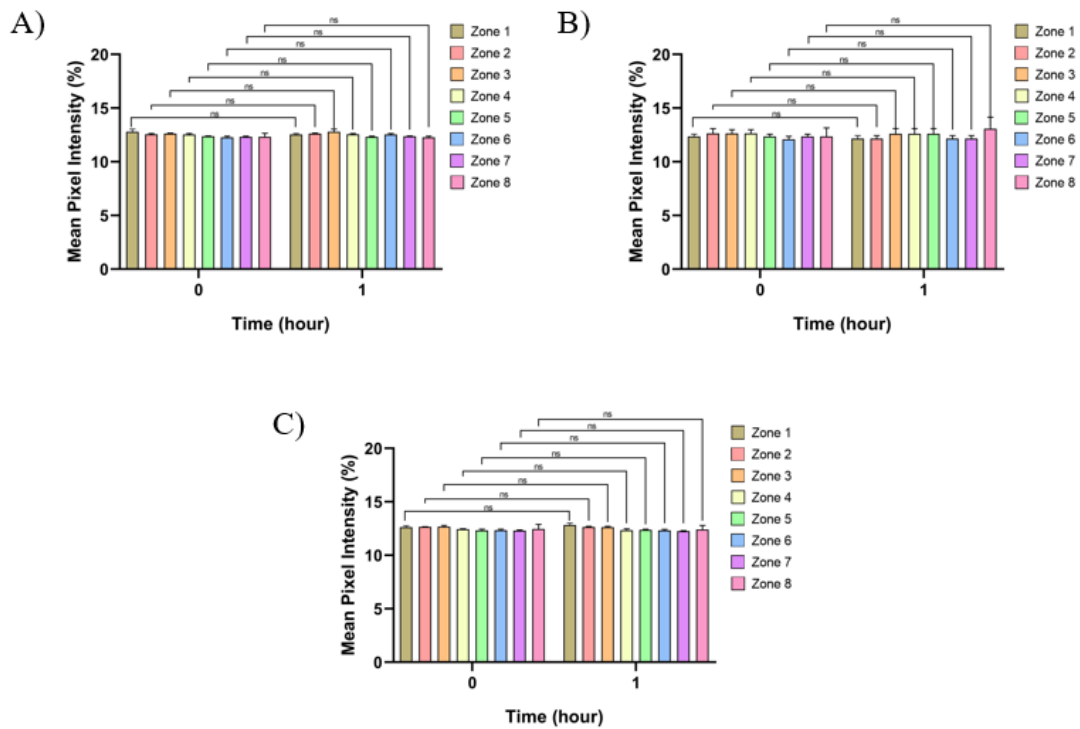


Figure 3.14. ImageJ analysis of the 8 zones of the chip Before and after centrifuging PBS used as control for 60 min at 9000 rpm. Zone 1 represents the top of the channel and zone 8 represents the bottom of the channel. A) ImageJ analysis for 50 nm particles. B) ImageJ analysis for 100 nm particles. C) ImageJ analysis for 200 nm particles. ****, *** and ns indicate $p < 0.0001$, $p < 0.001$, and $p > 0.05$ respectively.

3.6.2. Enrichment of Nanoparticles at the Bottom of the Channel

To determine the time it takes for particles of varied sizes to reach saturation at the bottom of the channel, noise values of PBS were subtracted by measuring the fluorescence intensity values of the channel bottom over time (Figure 3.15). It was observed that 200 nm particles reached 95% saturation at the end of 15 min, 100 nm particles reached 95% saturation at the end of 25 min, and 50 nm particles reached approximately 90% saturation at the end of 60 min.

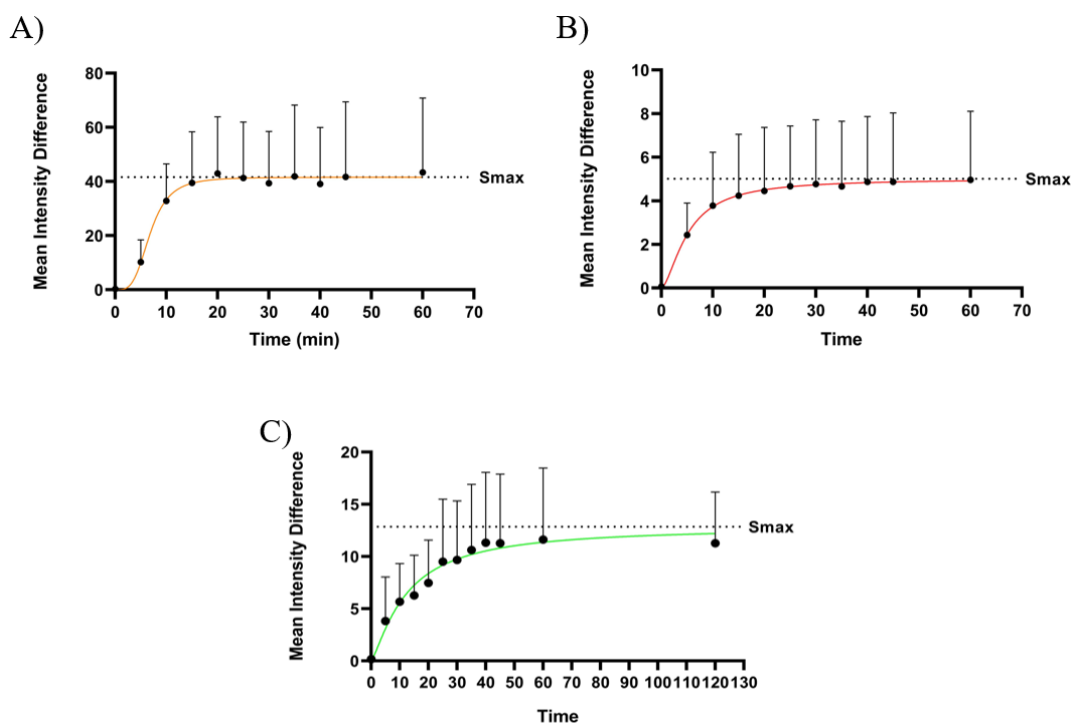


Figure 3.15. Change of mean intensity value of the channel bottom depending on time (mean intensity value of PBS noise is subtracted). A) 200 nm particles. B) 100 nm particles. C) 50 nm particles. Smax represents 100% saturation.

3.6.3. Collection of Enriched Nanoparticles

To observe whether the particles collected at the bottom of the channel could be successfully collected from within the chip, particles of 200 nm size were centrifuged at 9000 rpm for 20 minutes. The bottom of the channel and the parts where outlet 1 and 2 are located were examined under a fluorescence microscope (Figure 3.16). At the end of 20 minutes, it was observed that 200 nm particles were successfully isolated at the bottom of the channel and there were no particles in the section where outlet 1 was located. Outlet 1 was broken and the remaining liquid (50 μ L) at the top of the channel was collected. Then, outlet 2 was broken and the particles at the bottom of the channel were collected (10 μ L). When the channel was examined under the microscope again, it was observed that there was no radiation at the bottom of the channel and the particles could be collected successfully from the bottom of the channel.



Figure 3.16. Fluorescence microscope images of the isolated particles before and after collection from the channel.

3.6.4. Isolation of Exosomes

Since exosome sizes vary between 30-150 nm, 60 min at 9000 rpm were chosen to be used in the isolation of exosomes to ensure over 90% collection of exosomes. The exosome sample isolated from the commercial kit and the conditioned medium sample were scanned under a confocal microscope after being centrifuged at 9000 rpm for 60 min (Figure 3.17). In both samples, while no signal was observed at the bottom of the channel before centrifugation, exosomes were observed to accumulate after centrifugation.

In addition, the entire channel was scanned under the confocal microscope and the mean intensity value of the signal difference at the bottom and top of the channel was measured (Figure 3.18). A statistical difference was observed at the channel bottom in both samples ($p < 0.001$ for isolated exosome and $p < 0.01$ for conditioned medium).

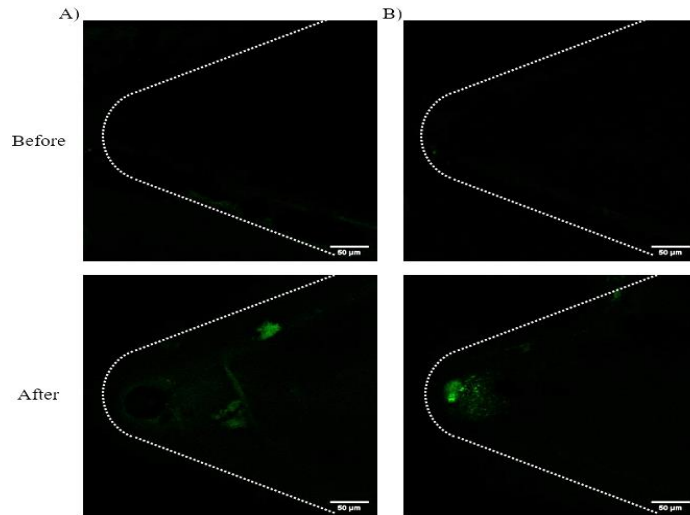


Figure 3.17. Images of the channel bottom under confocal microscopy before and after centrifugation. A) Isolated exosome sample from commercial kit. B) Conditioned medium sample.

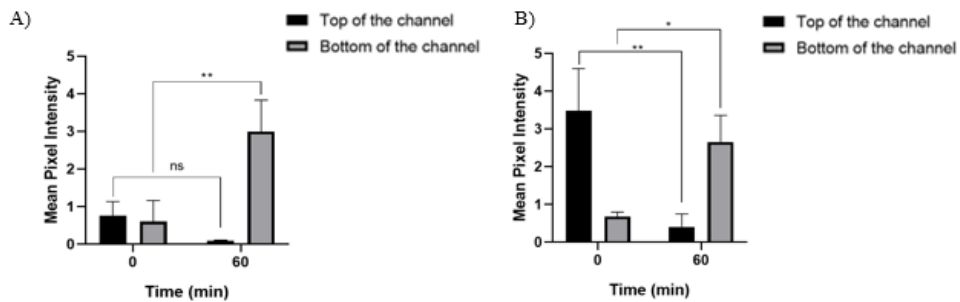


Figure 3.18. ImageJ analysis of the top and bottom of the chip before and after centrifuging for 60 min at 9000 rpm. A) Isolated exosome. B) Conditioned medium. **, * and ns indicate $p < 0.001$, $p < 0.01$, and $p > 0.05$ respectively.

Since the imaging of exosomes would be done using a confocal microscope, images of serum free medium (SFM) and PBS samples were taken before and after centrifugation to examine the difference between the top and bottom of the channel (Figure 3.19). When the mean intensity values of the channel before and after

centrifugation were compared with both controls, no statistical difference was observed ($p > 0.96$ for PBS and $p > 0.88$ for SFM medium).

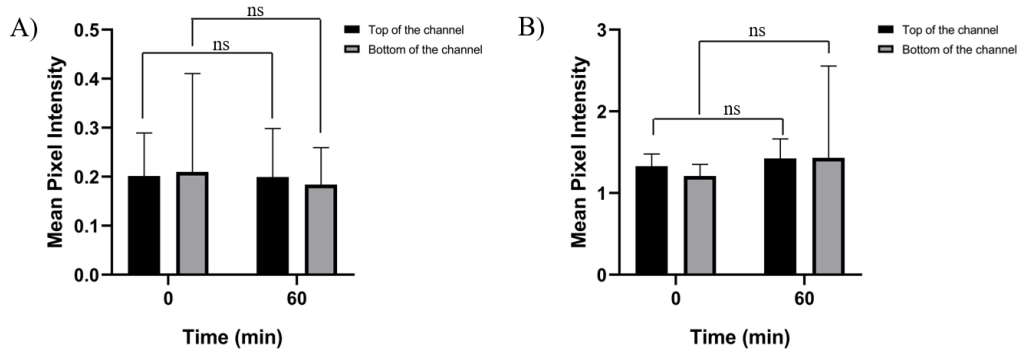


Figure 3.19. ImageJ analysis of the top and bottom of the chip before and after centrifuging for 60 min at 9000 rpm. A) Serum free medium. B) PBS. **, * and ns indicate $p < 0.001$, $p < 0.01$, and $p > 0.05$ respectively.

3.7. Conclusion

In this chapter, the isolation and enrichment of exosomes were achieved within 1 hour using a benchtop centrifuge device with a centrifugal microfluidic chip containing a dead-end channel. Exosomes, which vary in size between 30-150 nm and are a branch of extracellular vesicles, are nanovesicles released by cells and can be obtained from almost all biological fluids. Since they serve as cargo in the interaction between cells, they carry very important information due to the nucleic acids they contain. With the developing technology, IVDs have the potential to be used as biomarkers, especially in the early diagnosis of diseases such as cancer. However, there is no conventional method for the isolation and concentration of exosomes, and the methods used in the isolation of nanoparticles are low in efficiency and the equipment used is time consuming and expensive. Thanks to the developed chip, both isolation and concentration of exosomes from the cell medium were achieved by centrifuging them at 9000 rpm (9418 g) for 60 minutes. In addition, the collection of particles which is isolated at the bottom of the channel was achieved owing to the added outlets to the dead-end chip. With this method,

exosomes could be isolated in a low-cost, fast, and simple way. It is hoped that in the future the chip will be used in biological fluids, increasing the potential for using exosomes as biomarkers in IVDs.

CHAPTER 4

CONCLUSION

In this thesis, a novel PMMA-based fabrication strategy was presented to realize high strength PMMA-based microfluidic chip and this strategy was applied to fabricate a centrifugal microfluidic chip to isolate and enrich nanoparticles and exosomes.

The first part of the thesis introduced a fast, easy, durable, and low-cost fabrication technique for PMMA-based microfluidics utilizing pure acetone as both a surface enhancement and bonding agent. PMMA is a preferred material for microfluidic fabrication due to its transparency, low autofluorescence, and biocompatibility. However, traditional methods for creating microchannels on PMMA often result in increased surface roughness and defects due to the heat generated by laser cutters. These defects compromise transparency and disrupt laminar flow. The research presented in this thesis offers a novel solution by combining hot acetone treatment with heat treatment, allowing the engraved channel surfaces to self-heal and regain their original transparency, smoothness, and hydrophobicity. This method also uses acetone as a bonding agent, achieving bonding strength comparable to PMMA's tensile strength and ensuring an airtight seal.

The second part of the thesis focused on the isolation and enrichment of exosomes using a benchtop centrifuge device with a centrifugal microfluidic chip containing a dead-end channel. Exosomes, which are nanovesicles ranging from 30-150 nm, play a crucial role in cellular communication and have significant potential as biomarkers for the early detection of diseases such as cancer. Traditional methods for isolating and concentrating exosomes are often inefficient, time-consuming, and expensive. The developed chip allows for the isolation and concentration of exosomes from the cell medium by centrifuging at 9000 rpm (9418 g) for 60 minutes. This low-cost, rapid, and easy-to-use method provides a practical solution for the efficient isolation of exosomes. The capability to collect exosomes at the bottom of the channel enhances the usability of the

chip, paving the way for its future application in biological fluids and increasing the potential for exosome-based diagnostics in IVDs.

The research presented in this thesis paves the way for several exciting future developments. There is significant potential for further optimization of the PMMA-based fabrication technique to enhance the precision and scalability of microfluidic devices. Expanding this method to more complex designs could make it suitable for advanced lab-on-a-chip systems and point-of-care diagnostics, potentially broadening its impact in various applications. Additionally, refining the centrifugal microfluidic chip developed for exosome isolation could lead to improvements in its efficiency and automation, making it applicable for isolating a wider range of extracellular vesicles and nanoparticles. Integrating these technologies into clinical settings through collaborations with medical researchers could advance exosome-based diagnostic assays, contributing to earlier disease detection and the development of personalized medicine approaches. Overall, these advancements hold the promise of significantly enhancing diagnostic capabilities and providing deeper insights into the role of extracellular vesicles in health and disease.

REFERENCES

1. Yang, J.; Cheng, Y.; Gong, X.; Yi, S.; Li, C.-W.; Jiang, L.; Yi, C. An Integrative Review on the Applications of 3D Printing in the Field of *in Vitro* Diagnostics. *Chinese Chemical Letters*. **2022**, *33* (5), 2231–2242. <https://doi.org/10.1016/j.ccllet.2021.08.105>.
2. Wang, L.; Xu, W.; Wang, B.; Si, X.; Li, S. Methods and Advances in the Design, Testing and Development of *In Vitro* Diagnostic Instruments. *Processes*. **2023**, *11* (2), 403. <https://doi.org/10.3390/pr11020403>.
3. Khosla, N. K.; Lesinski, J. M.; Colombo, M.; Bezinge, L.; deMello, A. J.; Richards, D. A. Simplifying the Complex: Accessible Microfluidic Solutions for Contemporary Processes within *in Vitro* Diagnostics. *Lab Chip*. **2022**, *22* (18), 3340–3360. <https://doi.org/10.1039/D2LC00609J>.
4. Martín, J.; Tena, N.; Asuero, A. G. Current State of Diagnostic, Screening and Surveillance Testing Methods for COVID-19 from an Analytical Chemistry Point of View. *Microchemical Journal*. **2021**, *167*, 106305. <https://doi.org/10.1016/j.microc.2021.106305>.
5. Wu, M.; Lai, Q.; Ju, Q.; Li, L.; Yu, H.-D.; Huang, W. Paper-Based Fluorogenic Devices for *in Vitro* Diagnostics. *Biosens Bioelectron*. **2018**, *102*, 256–266. <https://doi.org/10.1016/j.bios.2017.11.006>.
6. Liu, D.; Wang, Y.; Li, X.; Li, M.; Wu, Q.; Song, Y.; Zhu, Z.; Yang, C. Integrated Microfluidic Devices for *in Vitro* Diagnostics at Point of Care. *Aggregate*. **2022**, *3* (5). <https://doi.org/10.1002/agt2.184>.
7. Loo, J. F. C.; Ho, A. H. P.; Turner, A. P. F.; Mak, W. C. Integrated Printed Microfluidic Biosensors. *Trends Biotechnol*. **2019**, *37* (10), 1104–1120. <https://doi.org/10.1016/j.tibtech.2019.03.009>.
8. Ainla, A.; Mousavi, M. P. S.; Tsaloglou, M.-N.; Redston, J.; Bell, J. G.; Fernández-Abedul, M. T.; Whitesides, G. M. Open-Source Potentiostat for Wireless Electrochemical Detection with Smartphones. *Anal Chem*. **2018**, *90* (10), 6240–6246. <https://doi.org/10.1021/acs.analchem.8b00850>.

9. Karakuzu, B.; Anil İnevi, M.; Tarim, E. A.; Sarigil, O.; Guzelgulgen, M.; Kecili, S.; Cesmeli, S.; Koc, S.; Baslar, M. S.; Oksel Karakus, C.; Ozcivici, E.; Tekin, H. C. Magnetic Levitation-Based Miniaturized Technologies for Advanced Diagnostics. *Emergent Materials*. **2024**. <https://doi.org/10.1007/s42247-024-00762-6>.
10. Beltrán-García, J.; Osca-Verdegal, R.; Mena-Mollá, S.; García-Giménez, J. L. Epigenetic IVD Tests for Personalized Precision Medicine in Cancer. *Front Genet*. **2019**, *10*. <https://doi.org/10.3389/fgene.2019.00621>.
11. Wang, Z.; Wang, Q.; Qin, F.; Chen, J. Exosomes: A Promising Avenue for Cancer Diagnosis beyond Treatment. *Front Cell Dev Biol*. **2024**, *12*. <https://doi.org/10.3389/fcell.2024.1344705>.
12. Cheng, J.; Nonaka, T.; Wong, D. T. W. Salivary Exosomes as Nanocarriers for Cancer Biomarker Delivery. *Materials*. **2019**, *12* (4), 654. <https://doi.org/10.3390/ma12040654>.
13. Hu, Z.-L.; Li, H.-Y.; Chang, X.; Li, Y.-Y.; Liu, C.-H.; Gao, X.-X.; Zhai, Y.; Chen, Y.-X.; Li, C.-Q. Exosomes Derived from Stem Cells as an Emerging Therapeutic Strategy for Intervertebral Disc Degeneration. *World J Stem Cells*. **2020**, *12* (8), 803–813. <https://doi.org/10.4252/wjsc.v12.i8.803>.
14. Gao, J.; Li, A.; Hu, J.; Feng, L.; Liu, L.; Shen, Z. Recent Developments in Isolating Methods for Exosomes. *Front Bioeng Biotechnol*. **2023**, *10*. <https://doi.org/10.3389/fbioe.2022.1100892>.
15. Oksuz, C.; Tarim, E. A.; Ozcan, H. A.; Koc, S.; Tekin, H. C. Sample Preparation Using Microfluidic Technologies for Non-Invasive Tests. In Reference Module in Chemistry, Molecular Sciences and Chemical Engineering; Elsevier, 2024. <https://doi.org/10.1016/B978-0-443-15978-7.00038-2>.
16. Tarim, E. A.; Anil İnevi, M.; Ozkan, I.; Kecili, S.; Bilgi, E.; Baslar, M. S.; Oksel Karakus, C.; Tekin, H. C. Microfluidic-Based Technologies for Diagnosis, Prevention, and Treatment of COVID-19: Recent Advances and Future Directions. *Biomed Microdevices*. **2023**, *25* (2), 10. <https://doi.org/10.1007/s10544-023-00649-z>.
17. Tarim, E. A.; Karakuzu, B.; Oksuz, C.; Sarigil, O.; Kizilkaya, M.; Al-Ruweidi, M. K. A. A.; Yalcin, H. C.; Ozcivici, E.; Tekin, H. C. Microfluidic-Based Virus Detection Methods for Respiratory Diseases. *Emergent Materials*. **2021**, *4* (1), 143–168. <https://doi.org/10.1007/s42247-021-00169-7>.

18. Tekin, H. C.; Gijs, M. A. M. Ultrasensitive Protein Detection: A Case for Microfluidic Magnetic Bead-Based Assays. *Lab Chip*, **2013**, *13* (24), 4711. <https://doi.org/10.1039/c3lc50477h>.
19. Sant, S.; Tao, S. L.; Fisher, O. Z.; Xu, Q.; Peppas, N. A.; Khademhosseini, A. Microfabrication Technologies for Oral Drug Delivery. *Adv Drug Deliv Rev.* **2012**, *64* (6), 496–507. <https://doi.org/10.1016/j.addr.2011.11.013>.
20. Zhang, Y.; Li, J.; Jiao, S.; Li, Y.; Zhou, Y.; Zhang, X.; Maryam, B.; Liu, X. Microfluidic Sensors for the Detection of Emerging Contaminants in Water: A Review. *Science of The Total Environment.* **2024**, *929*, 172734. <https://doi.org/10.1016/j.scitotenv.2024.172734>.
21. Bashir, R. BioMEMS: State-of-the-Art in Detection, Opportunities and Prospects. *Adv Drug Deliv Rev.* **2004**, *56* (11), 1565–1586. <https://doi.org/10.1016/j.addr.2004.03.002>.
22. de Mello, A. J.; Beard, N. Focus. Dealing with ‘Real’ Samples: Sample Pre-Treatment in Microfluidic Systems. *Lab Chip.* **2003**, *3* (1), 11N-20N. <https://doi.org/10.1039/B301019H>.
23. Iria, I.; Soares, R. R. G.; Brás, E. J. S.; Chu, V.; Gonçalves, J.; Conde, J. P. Accurate and Rapid Microfluidic ELISA to Monitor Infliximab Titers in Patients with Inflammatory Bowel Diseases. *Analyst.* **2022**, *147* (3), 480–488. <https://doi.org/10.1039/D1AN01810H>.
24. Yang, B.; Wang, P.; Li, Z.; Tao, C.; You, Q.; Sekine, S.; Zhuang, S.; Zhang, D.; Yamaguchi, Y. A Continuous Flow PCR Array Microfluidic Chip Applied for Simultaneous Amplification of Target Genes of Periodontal Pathogens. *Lab Chip.* **2022**, *22* (4), 733–737. <https://doi.org/10.1039/D1LC00814E>.
25. Brennan, D.; O’Connor, L.; Cormican, M.; Kileen, J.; Clancy, E.; Smith, T. J.; Galvin, P. Development of a Disposable Cartridge Real-Time PCR Test for Detection of Chlamydia Trachomatis Directly from Urine. *Sens Actuators B Chem.* **2021**, *339*, 129873. <https://doi.org/10.1016/j.snb.2021.129873>.
26. Arias-Alpizar, K.; Sánchez-Cano, A.; Prat-Trunas, J.; de la Serna Serna, E.; Alonso, O.; Sulleiro, E.; Sánchez-Montalvá, A.; Diéguez, A.; Baldrich, E. Malaria Quantitative POC Testing Using Magnetic Particles, a Paper Microfluidic Device and a Hand-Held Fluorescence Reader. *Biosens Bioelectron.* **2022**, *215*, 114513. <https://doi.org/10.1016/j.bios.2022.114513>.

27. Carvalho, D. J.; Kip, A. M.; Romitti, M.; Nazzari, M.; Tegel, A.; Stich, M.; Krause, C.; Caiment, F.; Costagliola, S.; Moroni, L.; Giselbrecht, S. Thyroid-on-a-Chip: An Organoid Platform for In Vitro Assessment of Endocrine Disruption. *Adv Healthc Mater.* **2023**, *12* (8). <https://doi.org/10.1002/adhm.202201555>.
28. Cai, G.; Huang, Y.; Chen, B.; Shen, Y.; Shi, X.; Peng, B.; Mi, S.; Huang, J. Modular Design of Centrifugal Microfluidic System and Its Application in Nucleic Acid Screening. *Talanta.* **2023**, *259*, 124486. <https://doi.org/10.1016/j.talanta.2023.124486>.
29. Gharib, G.; Bütün, İ.; Munganlı, Z.; Kozalak, G.; Namlı, İ.; Sarraf, S. S.; Ahmadi, V. E.; Toyran, E.; van Wijnen, A. J.; Koşar, A. Biomedical Applications of Microfluidic Devices: A Review. *Biosensors (Basel).* **2022**, *12* (11), 1023. <https://doi.org/10.3390/bios12111023>.
30. Niculescu, A.-G.; Chircov, C.; Bîrcă, A. C.; Grumezescu, A. M. Fabrication and Applications of Microfluidic Devices: A Review. *Int J Mol Sci.* **2021**, *22* (4), 2011. <https://doi.org/10.3390/ijms22042011>.
31. Gorkin, R.; Park, J.; Siegrist, J.; Amasia, M.; Lee, B. S.; Park, J.-M.; Kim, J.; Kim, H.; Madou, M.; Cho, Y.-K. Centrifugal Microfluidics for Biomedical Applications. *Lab Chip.* **2010**, *10* (14), 1758. <https://doi.org/10.1039/b924109d>.
32. Clime, L.; Brassard, D.; Geissler, M.; Veres, T. Active Pneumatic Control of Centrifugal Microfluidic Flows for Lab-on-a-Chip Applications. *Lab Chip.* **2015**, *15* (11), 2400–2411. <https://doi.org/10.1039/C4LC01490A>.
33. Strohmeier, O.; Keller, M.; Schwemmer, F.; Zehnle, S.; Mark, D.; von Stetten, F.; Zengerle, R.; Paust, N. Centrifugal Microfluidic Platforms: Advanced Unit Operations and Applications. *Chem Soc Rev.* **2015**, *44* (17), 6187–6229. <https://doi.org/10.1039/C4CS00371C>.
34. Tang, M.; Wang, G.; Kong, S.-K.; Ho, H.-P. A Review of Biomedical Centrifugal Microfluidic Platforms. *Micromachines (Basel).* **2016**, *7* (2), 26. <https://doi.org/10.3390/mi7020026>.
35. Kong, L. X.; Perebikovskiy, A.; Moebius, J.; Kulinsky, L.; Madou, M. Lab-on-a-CD: A Fully Integrated Molecular Diagnostic System. *SLAS Technol.* **2016**, *21* (3), 323–355. <https://doi.org/10.1177/2211068215588456>.

36. Gilmore, J.; Islam, M.; Martinez-Duarte, R. Challenges in the Use of Compact Disc-Based Centrifugal Microfluidics for Healthcare Diagnostics at the Extreme Point of Care. *Micromachines (Basel)*. **2016**, *7* (4), 52. <https://doi.org/10.3390/mi7040052>.
37. Madadelahi, M.; Acosta-Soto, L. F.; Hosseini, S.; Martinez-Chapa, S. O.; Madou, M. J. Mathematical Modeling and Computational Analysis of Centrifugal Microfluidic Platforms: A Review. *Lab Chip*. **2020**, *20* (8), 1318–1357. <https://doi.org/10.1039/C9LC00775J>.
38. Nayak, S.; Blumenfeld, N. R.; Laksanasopin, T.; Sia, S. K. Point-of-Care Diagnostics: Recent Developments in a Connected Age. *Anal Chem*. **2017**, *89* (1), 102–123. <https://doi.org/10.1021/acs.analchem.6b04630>.
39. Martins, J. P.; Torrieri, G.; Santos, H. A. The Importance of Microfluidics for the Preparation of Nanoparticles as Advanced Drug Delivery Systems. *Expert Opin Drug Deliv*. **2018**, *15* (5), 469–479. <https://doi.org/10.1080/17425247.2018.1446936>.
40. Peeling, R. W.; Mabey, D. Point-of-Care Tests for Diagnosing Infections in the Developing World. *Clinical Microbiology and Infection*. **2010**, *16* (8), 1062–1069. <https://doi.org/10.1111/j.1469-0691.2010.03279.x>.
41. Nielsen, J. B.; Hanson, R. L.; Almughamsi, H. M.; Pang, C.; Fish, T. R.; Woolley, A. T. Microfluidics: Innovations in Materials and Their Fabrication and Functionalization. *Anal Chem*. **2020**, *92* (1), 150–168. <https://doi.org/10.1021/acs.analchem.9b04986>.
42. Fujii, T. PDMS-Based Microfluidic Devices for Biomedical Applications. *Microelectron Eng*. **2002**, *61–62*, 907–914. [https://doi.org/10.1016/S0167-9317\(02\)00494-X](https://doi.org/10.1016/S0167-9317(02)00494-X).
43. Roosa, C.; Pruet, L.; Trujillo, J.; Rodriguez, A.; Pfaff, B.; Cornell, N.; Flanagan, C.; Griffin, D. R. Microfluidic Synthesis of Microgel Building Blocks for Microporous Annealed Particle Scaffold. *Journal of Visualized Experiments*. **2022**, No. 184. <https://doi.org/10.3791/64119>.
44. Miranda, I.; Souza, A.; Sousa, P.; Ribeiro, J.; Castanheira, E. M. S.; Lima, R.; Minas, G. Properties and Applications of PDMS for Biomedical Engineering: A Review. *J Funct Biomater*. **2021**, *13* (1), 2. <https://doi.org/10.3390/jfb13010002>.

45. Tony, A.; Badea, I.; Yang, C.; Liu, Y.; Wells, G.; Wang, K.; Yin, R.; Zhang, H.; Zhang, W. The Additive Manufacturing Approach to Polydimethylsiloxane (PDMS) Microfluidic Devices: Review and Future Directions. *Polymers (Basel)*. **2023**, *15* (8), 1926. <https://doi.org/10.3390/polym15081926>.
46. Bohl, B.; Steger, R.; Zengerle, R.; Koltay, P. Multi-Layer SU-8 Lift-off Technology for Microfluidic Devices. *Journal of Micromechanics and Microengineering*. **2005**, *15* (6), 1125–1130. <https://doi.org/10.1088/0960-1317/15/6/002>.
47. Olatunji, O.; Das, D. B. Drug Delivery Using Microneedles. In *Comprehensive Biotechnology*; Elsevier, 2011; pp 625–642. <https://doi.org/10.1016/B978-0-08-088504-9.00501-8>.
48. Gale, B. K.; Jafek, A. R.; Lambert, C. J.; Goenner, B. L.; Moghimifam, H.; Nze, U. C.; Kamarapu, S. K. A Review of Current Methods in Microfluidic Device Fabrication and Future Commercialization Prospects. *Inventions*. **2018**, *3* (3), 60. <https://doi.org/10.3390/inventions3030060>.
49. Lee, J. N.; Jiang, X.; Ryan, D.; Whitesides, G. M. Compatibility of Mammalian Cells on Surfaces of Poly(Dimethylsiloxane). *Langmuir*. **2004**. <https://doi.org/10.1021/la048562>.
50. Fiorini, G. S.; Chiu, D. T. Disposable Microfluidic Devices: Fabrication, Function, and Application. *Biotechniques*. **2005**, *38* (3), 429–446. <https://doi.org/10.2144/05383RV02>.
51. Scott, S.; Ali, Z. Fabrication Methods for Microfluidic Devices: An Overview. *Micromachines (Basel)*. **2021**, *12* (3), 319. <https://doi.org/10.3390/mi12030319>.
52. Tsao, C.-W. Polymer Microfluidics: Simple, Low-Cost Fabrication Process Bridging Academic Lab Research to Commercialized Fabrication. *Micromachines (Basel)*. **2016**, *7* (12), 225. <https://doi.org/10.3390/mi7120225>.
53. Schulz, U. Review of Modern Techniques to Generate Antireflective Properties on Thermoplastic Polymers. *Appl Opt*. **2006**, *45* (7), 1608. <https://doi.org/10.1364/AO.45.001608>.
54. Shakeri, A.; Khan, S.; Jarad, N. A.; Didar, T. F. The Fabrication and Bonding of Thermoplastic Microfluidics: A Review. *Materials*. **2022**, *15* (18), 6478. <https://doi.org/10.3390/ma15186478>.

55. Chen, Y.; Zhang, L.; Chen, G. Fabrication, Modification, and Application of Poly(Methyl Methacrylate) Microfluidic Chips. *Electrophoresis*. **2008**, *29* (9), 1801–1814. <https://doi.org/10.1002/elps.200700552>.
56. van Midwoud, P. M.; Janse, A.; Merema, M. T.; Groothuis, G. M. M.; Verpoorte, E. Comparison of Biocompatibility and Adsorption Properties of Different Plastics for Advanced Microfluidic Cell and Tissue Culture Models. *Anal Chem*. **2012**, *84* (9), 3938–3944. <https://doi.org/10.1021/ac300771z>.
57. Damodara, S.; Shahriari, S.; Wu, W.-I.; Rezai, P.; Hsu, H.-H.; Selvaganapathy, R. Materials and Methods for Microfabrication of Microfluidic Devices. In *Microfluidic Devices for Biomedical Applications*; Elsevier, 2021; pp 1–78. <https://doi.org/10.1016/B978-0-12-819971-8.00008-1>.
58. Kim, M.; Moon, B.-U.; Hidrovo, C. H. Enhancement of the Thermo-Mechanical Properties of PDMS Molds for the Hot Embossing of PMMA Microfluidic Devices. *Journal of Micromechanics and Microengineering*. **2013**, *23* (9), 095024. <https://doi.org/10.1088/0960-1317/23/9/095024>.
59. Rowland, H. D.; Charest, J. L.; Wright, T. L.; King, W. P. Transport During Hot Embossing Micro-Manufacturing Studied via Stylus Profilometry and SEM. In *Heat Transfer, Volume 3*; ASME/EDC, 2003; pp 169–176. <https://doi.org/10.1115/IMECE2003-41838>.
60. Jeon, J. S.; Chung, S.; Kamm, R. D.; Charest, J. L. Hot Embossing for Fabrication of a Microfluidic 3D Cell Culture Platform. *Biomed Microdevices*. **2011**, *13* (2), 325–333. <https://doi.org/10.1007/s10544-010-9496-0>.
61. Wiriyakun, N.; Nacapricha, D.; Chantiwas, R. A Simple Method Using Two-Step Hot Embossing Technique with Shrinking for Fabrication of Cross Microchannels on PMMA Substrate and Its Application to Electrophoretic Separation of Amino Acids in Functional Drinks. *Talanta*. **2016**, *161*, 574–582. <https://doi.org/10.1016/j.talanta.2016.09.001>.
62. Chen, C.-S.; Chen, S.-C.; Liao, W.-H.; Chien, R.-D.; Lin, S.-H. Micro Injection Molding of a Micro-Fluidic Platform. *International Communications in Heat and Mass Transfer*. **2010**, *37* (9), 1290–1294. <https://doi.org/10.1016/j.icheatmasstransfer.2010.06.032>.

63. McCormick, R. M.; Nelson, R. J.; Alonso-Amigo, M. G.; Benvegna, D. J.; Hooper, H. H. Microchannel Electrophoretic Separations of DNA in Injection-Molded Plastic Substrates. *Anal Chem.* **1997**, *69* (14), 2626–2630. <https://doi.org/10.1021/ac9701997>.
64. Ma, X.; Li, R.; Jin, Z.; Fan, Y.; Zhou, X.; Zhang, Y. Injection Molding and Characterization of PMMA-Based Microfluidic Devices. *Microsystem Technologies.* **2020**, *26* (4), 1317–1324. <https://doi.org/10.1007/s00542-019-04662-2>.
65. Frizelle, W. G. Injection Molding Technology. In *Applied Plastics Engineering Handbook*; Elsevier, 2011; pp 205–214. <https://doi.org/10.1016/B978-1-4377-3514-7.10013-3>.
66. Behroodi, E.; Latifi, H.; Bagheri, Z.; Ermis, E.; Roshani, S.; Salehi Moghaddam, M. A Combined 3D Printing/CNC Micro-Milling Method to Fabricate a Large-Scale Microfluidic Device with the Small Size 3D Architectures: An Application for Tumor Spheroid Fabrication. *Sci Rep.* **2020**, *10* (1), 22171. <https://doi.org/10.1038/s41598-020-79015-5>.
67. Wu, W.; Trinh, K. T. L.; Zhang, Y.; Yoon Lee, N. Portable Plastic Syringe as a Self-Actuated Pump for Long-Distance Uniform Delivery of Liquid inside a Microchannel and Its Application for Flow-through Polymerase Chain Reaction on Chip. *RSC Adv.* **2015**, *5* (16), 12071–12077. <https://doi.org/10.1039/C4RA15473H>.
68. Dudala, S.; Rao, L. T.; Dubey, S. K.; Javed, A.; Goel, S. Experimental Characterization to Fabricate CO₂ Laser Ablated PMMA Microchannel with Homogeneous Surface. *Mater Today Proc.* **2020**, *28*, 804–807. <https://doi.org/10.1016/j.matpr.2019.12.302>.
69. Ravi-Kumar, S.; Lies, B.; Zhang, X.; Lyu, H.; Qin, H. Laser Ablation of Polymers: A Review. *Polym Int.* **2019**, *68* (8), 1391–1401. <https://doi.org/10.1002/pi.5834>.
70. Chen, L.; Yang, C.; Xiao, Y.; Yan, X.; Hu, L.; Eggersdorfer, M.; Chen, D.; Weitz, D. A.; Ye, F. Millifluidics, Microfluidics, and Nanofluidics: Manipulating Fluids at Varying Length Scales. *Mater Today Nano.* **2021**, *16*, 100136. <https://doi.org/10.1016/j.mtnano.2021.100136>.
71. Romoli, L.; Tantussi, G.; Dini, G. Experimental Approach to the Laser Machining of PMMA Substrates for the Fabrication of Microfluidic Devices. *Opt Lasers Eng.* **2011**, *49* (3), 419–427. <https://doi.org/10.1016/j.optlaseng.2010.11.013>.

72. Suriano, R.; Kuznetsov, A.; Eaton, S. M.; Kiyan, R.; Cerullo, G.; Osellame, R.; Chichkov, B. N.; Levi, M.; Turri, S. Femtosecond Laser Ablation of Polymeric Substrates for the Fabrication of Microfluidic Channels. *Appl Surf Sci.* **2011**, *257* (14), 6243–6250. <https://doi.org/10.1016/j.apsusc.2011.02.053>.
73. Wang, Z. K.; Zheng, H. Y.; Lim, R. Y. H.; Wang, Z. F.; Lam, Y. C. Improving Surface Smoothness of Laser-Fabricated Microchannels for Microfluidic Application. *Journal of Micromechanics and Microengineering.* **2011**, *21* (9), 095008. <https://doi.org/10.1088/0960-1317/21/9/095008>.
74. Matellan, C.; del Río Hernández, A. E. Cost-Effective Rapid Prototyping and Assembly of Poly(Methyl Methacrylate) Microfluidic Devices. *Sci Rep.* **2018**, *8* (1), 6971. <https://doi.org/10.1038/s41598-018-25202-4>.
75. Ogilvie, I. R. G.; Sieben, V. J.; Floquet, F. A.; Zmijan, R.; Mowlem, M. C.; Morgan, H. *SOLVENT PROCESSING OF PMMA AND COC CHIPS FOR BONDING DEVICES WITH OPTICAL QUALITY SURFACES*; 2010.
76. Becker, H.; Gärtner, C. Polymer Microfabrication Methods for Microfluidic Analytical Applications. *Electrophoresis.* **2000**, *21* (1), 12–26. [https://doi.org/10.1002/\(SICI\)1522-2683\(20000101\)21:1<12::AID-ELPS12>3.0.CO;2-7](https://doi.org/10.1002/(SICI)1522-2683(20000101)21:1<12::AID-ELPS12>3.0.CO;2-7).
77. Borók, A.; Laboda, K.; Bonyár, A. PDMS Bonding Technologies for Microfluidic Applications: A Review. *Biosensors (Basel).* **2021**, *11* (8), 292. <https://doi.org/10.3390/bios11080292>.
78. Welle, A.; Gottwald, E. UV-Based Patterning of Polymeric Substrates for Cell Culture Applications. *Biomed Microdevices.* **2002**, *4* (1), 33–41. <https://doi.org/10.1023/A:1014267712144>.
79. Bamshad, A.; Nikfarjam, A.; Khaleghi, H. A New Simple and Fast Thermally-Solvent Assisted Method to Bond PMMA–PMMA in Micro-Fluidics Devices. *Journal of Micromechanics and Microengineering.* **2016**, *26* (6), 065017. <https://doi.org/10.1088/0960-1317/26/6/065017>.
80. Li, J.; Chen, D.; Chen, G. Low-Temperature Thermal Bonding of PMMA Microfluidic Chips. *Anal Lett.* **2005**, *38* (7), 1127–1136. <https://doi.org/10.1081/AL-200057209>.

81. Hsu, Y.-C.; Chen, T.-Y. Applying Taguchi Methods for Solvent-Assisted PMMA Bonding Technique for Static and Dynamic μ -TAS Devices. *Biomed Microdevices*. **2007**, *9* (4), 513–522. <https://doi.org/10.1007/s10544-007-9059-1>.
82. Patra, N.; Barone, A. C.; Salerno, M. Solvent Effects on the Thermal and Mechanical Properties of Poly(Methyl Methacrylate) Casted from Concentrated Solutions. *Advances in Polymer Technology*. **2011**, *30* (1), 12–20. <https://doi.org/10.1002/adv.20203>.
83. Ng, S. P.; Wiria, F. E.; Tay, N. B. Low Distortion Solvent Bonding of Microfluidic Chips. *Procedia Eng.* **2016**, *141*, 130–137. <https://doi.org/10.1016/j.proeng.2015.09.212>.
84. Faghieh, M. M.; Sharp, M. K. Solvent-Based Bonding of PMMA–PMMA for Microfluidic Applications. *Microsystem Technologies*. **2019**, *25* (9), 3547–3558. <https://doi.org/10.1007/s00542-018-4266-7>.
85. Madadi, M.; Madadi, A.; Zareifar, R.; Nikfarjam, A. A Simple Solvent-Assisted Method for Thermal Bonding of Large-Surface, Multilayer PMMA Microfluidic Devices. *Sens Actuators A Phys.* **2023**, *349*, 114077. <https://doi.org/10.1016/j.sna.2022.114077>.
86. Trinh, K. T. L.; Thai, D. A.; Chae, W. R.; Lee, N. Y. Rapid Fabrication of Poly(Methyl Methacrylate) Devices for Lab-on-a-Chip Applications Using Acetic Acid and UV Treatment. *ACS Omega*. **2020**, *5* (28), 17396–17404. <https://doi.org/10.1021/acsomega.0c01770>.
87. Hassanpour-Tamrin, S.; Sanati-Nezhad, A.; Sen, A. A Simple and Low-Cost Approach for Irreversible Bonding of Polymethylmethacrylate and Polydimethylsiloxane at Room Temperature for High-Pressure Hybrid Microfluidics. *Sci Rep*. **2021**, *11* (1), 4821. <https://doi.org/10.1038/s41598-021-83011-8>.
88. Inan, H.; Kingsley, J. L.; Ozen, M. O.; Tekin, H. C.; Hoerner, C. R.; Imae, Y.; Metzner, T. J.; Preiss, J. S.; Durmus, N. G.; Ozsoz, M.; Wakelee, H.; Fan, A. C.; Tüzel, E.; Demirci, U. Monitoring Neutropenia for Cancer Patients at the Point of Care. *Small Methods*. **2017**, *1* (9). <https://doi.org/10.1002/smt.201700193>.
89. Paoli, R.; Di Giuseppe, D.; Badiola-Mateos, M.; Martinelli, E.; Lopez-Martinez, M. J.; Samitier, J. Rapid Manufacturing of Multilayered Microfluidic Devices for Organ on a Chip Applications. *Sensors*. **2021**, *21* (4), 1382. <https://doi.org/10.3390/s21041382>.

90. Li, J.; Liang, C.; Zhang, H.; Liu, C. Reliable and High Quality Adhesive Bonding for Microfluidic Devices. *Micro Nano Lett.* **2017**, *12* (2), 90–94. <https://doi.org/10.1049/mnl.2016.0478>.
91. Tsao, C.-W.; Chang, C.-Y.; Chien, P.-Y. Microwave-Assisted Solvent Bonding for Polymethyl Methacrylate Microfluidic Device. *Micromachines (Basel)*. **2022**, *13* (7), 1131. <https://doi.org/10.3390/mi13071131>.
92. Rahbar, M.; Chhina, S.; Sameoto, D.; Parameswaran, M. Microwave-Induced, Thermally Assisted Solvent Bonding for Low-Cost PMMA Microfluidic Devices. *Journal of Micromechanics and Microengineering*. **2010**, *20* (1), 015026. <https://doi.org/10.1088/0960-1317/20/1/015026>.
93. Toossi, A.; Moghadas, H.; Shayegh, M.; Sameoto, D.; Daneshmand, M. Efficient Microwave Susceptor Design for Localized Heating on Substrate. *IEEE Trans Compon Packaging Manuf Technol.* **2015**, *5* (4), 570–578. <https://doi.org/10.1109/TCPMT.2015.2409791>.
94. Hajduk, B.; Bednarski, H.; Jarka, P.; Janeczek, H.; Godzierz, M.; Tański, T. Thermal and Optical Properties of PMMA Films Reinforced with Nb₂O₅ Nanoparticles. *Sci Rep.* **2021**, *11* (1). <https://doi.org/10.1038/s41598-021-01282-7>.
95. Modena, M. M.; Rühle, B.; Burg, T. P.; Wuttke, S. Nanoparticle Characterization: What to Measure? *Advanced Materials*. **2019**, *31* (32). <https://doi.org/10.1002/adma.201901556>.
96. Schwirn, K.; Tietjen, L.; Beer, I. Why Are Nanomaterials Different and How Can They Be Appropriately Regulated under REACH? *Environ Sci Eur.* **2014**, *26* (1), 4. <https://doi.org/10.1186/2190-4715-26-4>.
97. Xie, Y.; Rufo, J.; Zhong, R.; Rich, J.; Li, P.; Leong, K. W.; Huang, T. J. Microfluidic Isolation and Enrichment of Nanoparticles. *ACS Nano*. **2020**, *14* (12), 16220–16240. <https://doi.org/10.1021/acsnano.0c06336>.
98. Mekuye, B.; Abera, B. Nanomaterials: An Overview of Synthesis, Classification, Characterization, and Applications. *Nano Select.* **2023**, *4* (8), 486–501. <https://doi.org/10.1002/nano.202300038>.
99. Doyle, L.; Wang, M. Overview of Extracellular Vesicles, Their Origin, Composition, Purpose, and Methods for Exosome Isolation and Analysis. *Cells*. **2019**, *8* (7), 727. <https://doi.org/10.3390/cells8070727>.

100. Abels, E. R.; Breakefield, X. O. Introduction to Extracellular Vesicles: Biogenesis, RNA Cargo Selection, Content, Release, and Uptake. *Cell Mol Neurobiol.* **2016**, *36* (3), 301–312. <https://doi.org/10.1007/s10571-016-0366-z>.
101. Bongiovanni, L.; Andriessen, A.; Wauben, M. H. M.; Hoen, E. N. M. N.-'t; de Bruin, A. Extracellular Vesicles: Novel Opportunities to Understand and Detect Neoplastic Diseases. *Vet Pathol.* **2021**, *58* (3), 453–471. <https://doi.org/10.1177/0300985821999328>.
102. Liga, A.; Vliegthart, A. D. B.; Oosthuyzen, W.; Dear, J. W.; Kersaudy-Kerhoas, M. Exosome Isolation: A Microfluidic Road-Map. *Lab Chip* **2015**, *15* (11), 2388–2394. <https://doi.org/10.1039/C5LC00240K>.
103. Kowal, J.; Tkach, M.; Théry, C. Biogenesis and Secretion of Exosomes. *Curr Opin Cell Biol.* **2014**, *29*, 116–125. <https://doi.org/10.1016/j.ceb.2014.05.004>.
104. Skog, J.; Würdinger, T.; van Rijn, S.; Meijer, D. H.; Gainche, L.; Curry, W. T.; Carter, B. S.; Krichevsky, A. M.; Breakefield, X. O. Glioblastoma Microvesicles Transport RNA and Proteins That Promote Tumour Growth and Provide Diagnostic Biomarkers. *Nat Cell Biol.* **2008**, *10* (12), 1470–1476. <https://doi.org/10.1038/ncb1800>.
105. Yang, X.; Weng, Z.; Mendrick, D. L.; Shi, Q. Circulating Extracellular Vesicles as a Potential Source of New Biomarkers of Drug-Induced Liver Injury. *Toxicol Lett.* **2014**, *225* (3), 401–406. <https://doi.org/10.1016/j.toxlet.2014.01.013>.
106. Xu, M.; Ji, J.; Jin, D.; Wu, Y.; Wu, T.; Lin, R.; Zhu, S.; Jiang, F.; Ji, Y.; Bao, B.; Li, M.; Xu, W.; Xiao, M. The Biogenesis and Secretion of Exosomes and Multivesicular Bodies (MVBs): Intercellular Shuttles and Implications in Human Diseases. *Genes Dis.* **2023**, *10* (5), 1894–1907. <https://doi.org/10.1016/j.gendis.2022.03.021>.
107. Lin, H.; Shi, X.; Li, H.; Hui, J.; Liu, R.; Chen, Z.; Lu, Y.; Tan, W. Urinary Exosomal MiRNAs as Biomarkers of Bladder Cancer and Experimental Verification of Mechanism of MiR-93-5p in Bladder Cancer. *BMC Cancer.* **2021**, *21* (1), 1293. <https://doi.org/10.1186/s12885-021-08926-x>.
108. Wang, J.; Ma, P.; Kim, D. H.; Liu, B.-F.; Demirci, U. Towards Microfluidic-Based Exosome Isolation and Detection for Tumor Therapy. *Nano Today.* **2021**, *37*, 101066. <https://doi.org/10.1016/j.nantod.2020.101066>.

109. Gurunathan, S.; Kang, M.-H.; Jeyaraj, M.; Qasim, M.; Kim, J.-H. Review of the Isolation, Characterization, Biological Function, and Multifarious Therapeutic Approaches of Exosomes. *Cells*. **2019**, *8* (4), 307. <https://doi.org/10.3390/cells8040307>.
110. Weaver, J. W.; Zhang, J.; Rojas, J.; Musich, P. R.; Yao, Z.; Jiang, Y. The Application of Exosomes in the Treatment of Triple-Negative Breast Cancer. *Front Mol Biosci*. **2022**, *9*. <https://doi.org/10.3389/fmolb.2022.1022725>.
111. Afridi, W. A.; Strachan, S.; Kasetsirikul, S.; Pannu, A. S.; Soda, N.; Gough, D.; Nguyen, N.-T.; Shiddiky, M. J. A. Potential Avenues for Exosomal Isolation and Detection Methods to Enhance Small-Cell Lung Cancer Analysis. *ACS Measurement Science Au*. **2023**, *3* (3), 143–161. <https://doi.org/10.1021/acsmesuresciau.2c00068>.
112. Chavda, V. P.; Pandya, A.; Kumar, L.; Raval, N.; Vora, L. K.; Pulakkat, S.; Patravale, V.; Salwa; Duo, Y.; Tang, B. Z. Exosome Nanovesicles: A Potential Carrier for Therapeutic Delivery. *Nano Today*. **2023**, *49*, 101771. <https://doi.org/10.1016/j.nantod.2023.101771>.
113. Butreddy, A.; Kommineni, N.; Dudhipala, N. Exosomes as Naturally Occurring Vehicles for Delivery of Biopharmaceuticals: Insights from Drug Delivery to Clinical Perspectives. *Nanomaterials*. **2021**, *11* (6), 1481. <https://doi.org/10.3390/nano11061481>.
114. Kanwar, S. S.; Dunlay, C. J.; Simeone, D. M.; Nagrath, S. Microfluidic Device (ExoChip) for on-Chip Isolation, Quantification and Characterization of Circulating Exosomes. *Lab Chip*. **2014**, *14* (11), 1891–1900. <https://doi.org/10.1039/C4LC00136B>.
115. Verma, V.; Ryan, K. M.; Padrela, L. Fabrication and Isolation of Pharmaceutical Drug Nanoparticles. *Int J Pharm*. **2021**, *603*, 120708. <https://doi.org/10.1016/j.ijpharm.2021.120708>.
116. Jiang, G.; Yan, J.; Wang, G.; Dai, M.; Xu, C.; Wang, J. Effect of Nanoparticles Concentration on the Evaporation Characteristics of Biodiesel. *Appl Surf Sci*. **2019**, *492*, 150–156. <https://doi.org/10.1016/j.apsusc.2019.06.118>.
117. Greening, D. W.; Xu, R.; Ji, H.; Tauro, B. J.; Simpson, R. J. A Protocol for Exosome Isolation and Characterization: Evaluation of Ultracentrifugation, Density-Gradient Separation, and Immunoaffinity Capture Methods; 2015; pp 179–209. https://doi.org/10.1007/978-1-4939-2550-6_15.

118. Salafi, T.; Zeming, K. K.; Zhang, Y. Advancements in Microfluidics for Nanoparticle Separation. *Lab Chip*. **2017**, *17* (1), 11–33. <https://doi.org/10.1039/C6LC01045H>.
119. Mori, Y. Size-Selective Separation Techniques for Nanoparticles in Liquid. *KONA Powder and Particle Journal*. **2015**, *32* (0), 102–114. <https://doi.org/10.14356/kona.2015023>.
120. Hanauer, M.; Pierrat, S.; Zins, I.; Lotz, A.; Sönnichsen, C. Separation of Nanoparticles by Gel Electrophoresis According to Size and Shape. *Nano Lett*. **2007**, *7* (9), 2881–2885. <https://doi.org/10.1021/nl071615y>.
121. Xu, X.; Cölfen, H. Ultracentrifugation Techniques for the Ordering of Nanoparticles. *Nanomaterials*. **2021**, *11* (2), 333. <https://doi.org/10.3390/nano11020333>.
122. Akbulut, O.; Mace, C. R.; Martinez, R. V.; Kumar, A. A.; Nie, Z.; Patton, M. R.; Whitesides, G. M. Separation of Nanoparticles in Aqueous Multiphase Systems through Centrifugation. *Nano Lett*. **2012**, *12* (8), 4060–4064. <https://doi.org/10.1021/nl301452x>.
123. Sweeney, S. F.; Woehrle, G. H.; Hutchison, J. E. Rapid Purification and Size Separation of Gold Nanoparticles via Diafiltration. *J Am Chem Soc*. **2006**, *128* (10), 3190–3197. <https://doi.org/10.1021/ja0558241>.
124. Jorgenson, J. W. Chromatography: Fundamentals and Applications of Chromatography and Related Differential Migration Methods, Part A: Fundamentals and Techniques, 6th Ed. Journal of Chromatography Library, Volume 69A Edited by Erich Heftmann (Orinda, CA). Elsevier B. V.: Amsterdam. 2004. XI + 544 Pp. \$245.00. ISBN 0-444-51107-5. *J Am Chem Soc*. **2005**, *127* (12), 4540–4541. <https://doi.org/10.1021/ja040972x>.
125. Wei, G.-T.; Liu, F.-K. Separation of Nanometer Gold Particles by Size Exclusion Chromatography. *J Chromatogr. A* **1999**, *836* (2), 253–260. [https://doi.org/10.1016/S0021-9673\(99\)00069-2](https://doi.org/10.1016/S0021-9673(99)00069-2).
126. Benfer, S.; Árki, P.; Tomandl, G. Ceramic Membranes for Filtration Applications — Preparation and Characterization. *Adv Eng Mater*. **2004**, *6* (7), 495–500. <https://doi.org/10.1002/adem.200400577>.

127. Van der Bruggen, B.; Mänttari, M.; Nyström, M. Drawbacks of Applying Nanofiltration and How to Avoid Them: A Review. *Sep Purif Technol.* **2008**, *63* (2), 251–263. <https://doi.org/10.1016/j.seppur.2008.05.010>.
128. Wang, C.-L.; Fang, M.; Xu, S.-H.; Cui, Y.-P. Salts-Based Size-Selective Precipitation: Toward Mass Precipitation of Aqueous Nanoparticles. *Langmuir.* **2010**, *26* (2), 633–638. <https://doi.org/10.1021/la903986v>.
129. Saunders, S. R.; Roberts, C. B. Size-Selective Fractionation of Nanoparticles at an Application Scale Using CO₂ Gas-Expanded Liquids. *Nanotechnology.* **2009**, *20* (47), 475605. <https://doi.org/10.1088/0957-4484/20/47/475605>.
130. Marassi, V.; Casolari, S.; Panzavolta, S.; Bonvicini, F.; Gentilomi, G. A.; Giordani, S.; Zattoni, A.; Reschiglian, P.; Roda, B. Synthesis Monitoring, Characterization and Cleanup of Ag-Polydopamine Nanoparticles Used as Antibacterial Agents with Field-Flow Fractionation. *Antibiotics.* **2022**, *11* (3), 358. <https://doi.org/10.3390/antibiotics11030358>.
131. Kapsch, A.; Farcet, M. R.; Wieser, A.; Ahmad, M. Q.; Miyabayashi, T.; Baylis, S. A.; Blümel, J.; Kreil, T. R. Antibody-enhanced Hepatitis E Virus Nanofiltration during the Manufacture of Human Immunoglobulin. *Transfusion (Paris).* **2020**, *60* (11), 2500–2507. <https://doi.org/10.1111/trf.16014>.
132. Houbart, V.; Fillet, M. Advances in Low Volume Sample Analysis Using Microfluidic Separation Techniques. In *Advances in Microfluidics - New Applications in Biology, Energy, and Materials Sciences*; InTech, 2016. <https://doi.org/10.5772/64952>.
133. Contreras-Naranjo, J. C.; Wu, H.-J.; Ugaz, V. M. Microfluidics for Exosome Isolation and Analysis: Enabling Liquid Biopsy for Personalized Medicine. *Lab Chip.* **2017**, *17* (21), 3558–3577. <https://doi.org/10.1039/C7LC00592J>.
134. Zhao, W.; Zhang, L.; Ye, Y.; Li, Y.; Luan, X.; Liu, J.; Cheng, J.; Zhao, Y.; Li, M.; Huang, C. Microsphere Mediated Exosome Isolation and Ultra-Sensitive Detection on a Dielectrophoresis Integrated Microfluidic Device. *Analyst.* **2021**, *146* (19), 5962–5972. <https://doi.org/10.1039/D1AN01061A>.
135. Woo, H.-K.; Sunkara, V.; Park, J.; Kim, T.-H.; Han, J.-R.; Kim, C.-J.; Choi, H.-I.; Kim, Y.-K.; Cho, Y.-K. Exodisc for Rapid, Size-Selective, and Efficient Isolation and Analysis of Nanoscale Extracellular Vesicles from Biological Samples. *ACS Nano.* **2017**, *11* (2), 1360–1370. <https://doi.org/10.1021/acsnano.6b06131>.

136. Yeo, J. C.; Kenry; Zhao, Z.; Zhang, P.; Wang, Z.; Lim, C. T. Label-Free Extraction of Extracellular Vesicles Using Centrifugal Microfluidics. *Biomicrofluidics*. **2018**, *12* (2). <https://doi.org/10.1063/1.5019983>.
137. Pishbin, E.; Eghbal, M.; Fakhari, S.; Kazemzadeh, A.; Navidbakhsh, M. The Effect of Moment of Inertia on the Liquids in Centrifugal Microfluidics. *Micromachines (Basel)*. **2016**, *7* (12), 215. <https://doi.org/10.3390/mi7120215>.
138. Hess, J. F.; Zehnle, S.; Juelg, P.; Hutzenlaub, T.; Zengerle, R.; Paust, N. Review on Pneumatic Operations in Centrifugal Microfluidics. *Lab Chip*. **2019**, *19* (22), 3745–3770. <https://doi.org/10.1039/C9LC00441F>.
139. Tan, Y. Z.; Zamani, F.; Tian, J.; Chew, J. W. Coriolis Effect Particles Segregator (CEPS): The Feasibility of Scaling up Lab-on-a-Chip Separation. *Microfluid Nanofluidics*. **2022**, *26* (2), 14. <https://doi.org/10.1007/s10404-022-02521-7>.
140. Alharbi, T. M. D.; Jellicoe, M.; Luo, X.; Vimalanathan, K.; Alsulami, I. K.; AL Harbi, B. S.; Igder, A.; Alrashaidi, F. A. J.; Chen, X.; Stubbs, K. A.; Chalker, J. M.; Zhang, W.; Boulos, R. A.; Jones, D. B.; Quinton, J. S.; Raston, C. L. Sub-Micron Moulding Topological Mass Transport Regimes in Angled Vortex Fluidic Flow. *Nanoscale Adv.* **2021**, *3* (11), 3064–3075. <https://doi.org/10.1039/D1NA00195G>.
141. Bayraktar, T.; Pidugu, S. B. Characterization of Liquid Flows in Microfluidic Systems. *Int J Heat Mass Transfer*. **2006**, *49* (5–6), 815–824. <https://doi.org/10.1016/j.ijheatmasstransfer.2005.11.007>.
142. Zehnle, S.; Schwemmer, F.; Roth, G.; von Stetten, F.; Zengerle, R.; Paust, N. Centrifugo-Dynamic Inward Pumping of Liquids on a Centrifugal Microfluidic Platform. *Lab Chip*. **2012**, *12* (24), 5142. <https://doi.org/10.1039/c2lc40942a>.
143. Olanrewaju, A.; Beaugrand, M.; Yafia, M.; Juncker, D. Capillary Microfluidics in Microchannels: From Microfluidic Networks to Capillary Circuits. *Lab Chip*. **2018**, *18* (16), 2323–2347. <https://doi.org/10.1039/C8LC00458G>.
144. Clime, L.; Daoud, J.; Brassard, D.; Malic, L.; Geissler, M.; Veres, T. Active Pumping and Control of Flows in Centrifugal Microfluidics. *Microfluid Nanofluidics* **2019**, *23* (3), 29. <https://doi.org/10.1007/s10404-019-2198-x>.
145. Öksüz, C. *Cell Separation in Microfluidic Devices*. M.S. Thesis, İzmir Institute of Technology, İzmir, 2022; p 1.